FNP

JOURNAL OF FOOD PROCESS ENGINEERING

D.R. HELDMAN
and
R.P. SINGH
COEDITORS

FOOD & NUTRITION PRESS, INC.

VOLUME 12, NUMBER 3

APRIL 1990

JOURNAL OF FOOD PROCESS ENGINEERING

All articles for publication and inquiries regarding publication should be sent to DR. D.R. HELDMAN, COEDITOR, *Journal of Food Process Engineering,* National Food Processors Association, 1401 New York Ave., N.W., Washington, D.C. 20005 USA: or DR. R.P. SINGH, COEDITOR, *Journal of Food Process Engineering,* University of California, Davis, Department of Agricultural Engineering, Davis, CA 95616 USA.

All subscriptions and inquiries regarding subscriptions should be sent to Food & Nutrition Press, Inc., 6527 Main Street, P.O. Box 374, Trumbull, CT 06611 USA.

One volume of four issues will be published annually. The price for Volume 12 is $92.00 which includes postage to U.S., Canada, and Mexico. Subscriptions to other countries are $109.00 per year via surface mail, and $118.00 per year via airmail.

Subscriptions for individuals for their own personal use are $72.00 for Volume 12 which includes postage to U.S., Canada, and Mexico. Personal subscriptions to other countries are $89.00 per year via surface mail, and $98.00 per year via airmail. Subscriptions for individuals should be sent direct to the publisher and marked for personal use.

The *Journal of Food Process Engineering* (ISSN: 0145-8876) is published quarterly (March, June, September and December) by Food & Nutrition Press, Inc.—Office of Publication is 6527 Main Street, P.O. Box 374, Trumbull, Connecticut 06611 USA.

Second class postage paid at Bridgeport, CT 06602.

POSTMASTER: Send address changes to Food & Nutrition Press, Inc., 6527 Main Street, P.O. Box 374, Trumbull, CT 06611.

JOURNAL OF FOOD PROCESS ENGINEERING

JOURNAL OF FOOD PROCESS ENGINEERING

Journal of
FOOD PROCESS ENGINEERING

VOLUME 12
NUMBER 3

Coeditors: D.R. HELDMAN
R.P. SINGH

FOOD & NUTRITION PRESS, INC.
TRUMBULL, CONNECTICUT 06611 USA

ISSN 0145-8876

Printed in the United States of America

CONTENTS

CENTERPOINT NUTRIENT DEGRADATION IN HEAT PROCESSED CONDUCTION HEATING FOOD MODEL

H. S. RAMASWAMY[1] and S. GHAZALA

Department of Food Science and Agricultural Chemistry
Department of Agricultural Engineering
Macdonald College of McGill University, Box 187
Ste. Anne de Bellevue, PQ, H9X 1C0, Canada

Accepted for Publication September 19, 1989

ABSTRACT

A methodology was developed for the evaluation of centerpoint nutrient degradation in conduction heating canned food subjected to thermal processing. The methodology involved sealing of 75 μL aliquote of test solution in a leakproof pressure-stable stainless steel capsule, placing the capsule at the geometric center of a can filled with a conduction heating simulated food prior to the closure, and recovering the capsule and analyzing the contents following a given thermal treatment. Experiments carried out using aqueous solutions of ascorbic acid and thiamine indicated good reproducibility of the results. Employing kinetic data for thermal destruction of the nutrients and center temperature-time history of the food simulant obtained from several simultaneously processed cans, the centerpoint nutrient retention predicted by several models agreed favorably with the experimental results.

INTRODUCTION

Controlled evaluation of nutrient destruction in thermo-processed foods is difficult mainly due to the lack of an efficient, heat stable and chemically inert conduction heating medium which can support uniform suspension of nutrients in its matrix for heat penetration tests and which enables efficient recovery of residual nutrients following the heat processing. Secondly, in terms of centerpoint destruction, it is difficult to isolate nutrients from specific test locations. Bentonite suspensions have been traditionally used to simulate heating behavior of foods (Adams *et al.* 1983; Ball and Olson 1957; Yamano 1976); while these are adequate to simulate heat transfer responses, nutrient dispersion in these suspensions and their subsequent recovery is a serious problem. Others have used

[1]To whom correspondence should be addressed.

compressed glasswool to form a three-dimensional matrix thereby restricting the mobility of water to simulate conduction heating conditions (Manji and van de Voort 1985). But studies in our laboratory have indicated that the compressed glasswool does not efficiently suppress convection currents, especially at higher temperatures.

Thermal processing is based on reducing the population, at the slowest heating point, of heat resistant microorganisms of public health concern to a level that is statistically considered satisfactory. In the case of conduction heating foods, each point in the cross section of a container receives a different thermal process than every other point. While from microbial standpoint the primary interest is achieving a minimal commercial sterility at the slowest heating point, it is the overall integrated lethal/destruction effect at every point in the container that is important when considering the nutrient retention. These studies have been carried out by numerous researchers, either employing finite difference/element computer simulations of the heat transfer process or by experimental techniques based on average destruction (Castillo *et al.* 1980; Downes and Hayakawa 1977; Holdsworth 1985; Jen *et al* 1971; Lenz and Lund 1980; Manson *et al.* 1970; Ohlsson 1980; Teixeira *et al.* 1969, 1975; Thijssen and Kochen 1980).

The biological validation methods (Hersom and Shore 1981; Hunter 1972; Pflug *et al.* 1980a,b) developed for verification of continuous aseptic processing operations employ a somewhat similar approach, but sample sizes in these studies are too large for approximating to a specific location. Rodriquez and Teixeira (1988) recently evaluated modified aluminum bio-indicator units (BIU's) which consisted of hollow cylindrical rods to contain a spore suspension. The aluminum rod was part of a two-part construction with the remaining part made of plastic to keep the sample section under thermal isolation from the can wall. Employing thermocouples, they showed that the contents of the aluminum rods followed the product temperature history (convection heating) very closely. There has been no published experimental correlation of computer simulated values for nutrient destruction at specific container locations during thermal processing of conduction heating foods.

The objective of this study is to establish a methodology to evaluate destruction of nutrients at the center of the container during thermal processing of conduction heating foods aimed at providing locational nutrient degradation data for verification of computer models.

MATERIALS AND METHODS

Test Samples

Test solutions containing two nutrients, ascorbic acid and thiamine, were prepared as follows in phosphate buffer (pH 4.05) double distilled water (DDW):

(1) Ascorbic acid in water: 20.0 g L-ascorbic acid dissolved in one L DDW, and (2) Thiamine in water: 2.0 g thiamine hydrochloride dissolved in one L DDW.

Test Capsules

The test capsules employed in the study were standard stainless steel differential scanning calorimetry sample pans from Perkin-Elmer Corporation, Norwalk, CT. The unit consisted of a stainless steel bottom pan to hold about 100 μL solution which could be crimp-sealed to a stainless steel cover with a rubber o-ring sandwiched in between to provide a pressure seal. The overall outside dimensions of the sealed capsule was 0.77 cm diameter $\times$ 0.29 cm height. This was considerably smaller than the BIU reported by Rodriguez and Teixeira (1988) which was an aluminum cylindrical rod of about 0.6 cm diameter and $\times$ 3.8 cm length. It should however be possible to reduce the dimensions of these BIU's to comparable levels.

Test Sample

A small volume (75 μL) of the prepared test solution (ascorbic acid and thiamine, taken separately) was introduced in to the stainless steel sample pan and crimp-sealed with a stainless steel cap with an o-ring at the capsule-cap interface. One such capsule was positioned at the geometric center of a conduction heating test can (size 211 $\times$ 400) prepared by carefully packing 85g acid washed celite (Sigma Chemical Co., St. Louis, MO) wetted with 180 mL water. Placing of the sample at the center posed no difficulties since wetted celite sample was dimensionally stable. In order to make sure the sample pan did not move during the test run, a small sheet of cotton mesh was placed about 1 cm below the pan to provide additional structural integrity to the wetted celite. Following a given test, these test pans were recovered, punctured with a sharp stainless steel needle and the samples analyzed for residual concentration of ascorbic acid/thiamine. Prior to removing the pan from the can, measurements were taken to make certain that it did not move from the geometric center.

Processing Conditions

Three time-temperature combinations were employed for thermal processing test runs: 115.6°C for 80 min; 121.1°C for 50 min and 126.7°C for 30 min. The retort come-up time was 10 min. Eight cans were used for each test run, four cans contained a capsule each with ascorbic acid and the other four contained capsules of thiamine. Additional test runs were carried out to evaluate the heat penetration characteristics (f_h, j_{ch}, f_c and j_{cc}) of the conduction heating food simulant (wetted celite) by positioning precalibrated copper-constantan thermocouples at the geometric center of the test cans.

Kinetic Data

The kinetics of thermal destruction of ascorbic acid and thiamine were obtained by heating aqueous samples (4 mL) in sealed in 10 mL glass ampoules in an oil bath for known time intervals at temperatures ranging from 110 to 150°C. The vitamin retention data were interpreted in terms of first-order reaction rate kinetics to obtain decimal reduction times (D values) at various temperatures and the temperature dependence of the kinetic parameters was obtained in terms of z value [negative reciprocal slope of D value (log scale) vs. temperature] using the TDT concept.

Estimation of Ascorbic Acid and Thiamine

Ascorbic acid and thiamine were estimated by a high pressure liquid chromatography technique using a Waters HPLC system (Waters Chromatography Division, Millipore Corp., Milford, MA) consisting of WISP Model 710B Intelligent Sample Processor, Model 510 HPLC Pump, Model 441 Absorbance Detector and a QA-1 Data Analysis System. The chromatography column was a u-Bondapak C18 (3.9 mm × 30 cm) stainless steel column with a Guard-Pak Precolumn (end capped) with a mobile phase of methanol:water (25:75 v/v) containing 20% low UV PIC B6 at a flow rate of 1 mL/min. The detector was set to 254 nm with 0.1 absorbance unit full scale and the sample injection was 15 μL. The retention times for ascorbic acid and thiamine were 3.10 and 9.00 min, respectively. The data processor was programmed to print the areas for the test peaks for ascorbic acid (3.10 min) and thiamine (9.00 min) directly based on previously stored calibration values using standard test solutions of ascorbic acid and thiamine.

Computer Predictions

Kinetic parameters of ascorbic acid and thiamine degradation (D and z values), heat penetration parameters evaluated experimentally (f_h, j_{ch}, f_c and j_{cc}) and the corresponding processing conditions (retort temperature, initial temperature, cooling water temperature, process time) were used in simple computer models based on (1) the original Ball's formula method (Ball 1923), (2) a modified Ball's formula method adopting an initial hyperbolic temperature response followed by a logarithmic response at the beginning of both heating and cooling sections (Finnegan 1984) and (3) a finite difference computer program (Teixeira *et al.* 1969) using a 10 × 10 spatial matrix and a 0.125 min time step to predict the retention of the above nutrients at the can center and the predicted values were compared with the experimental retention values.

RESULTS AND DISCUSSION

Centerpoint Nutrient Retention

The centerpoint retention of ascorbic acid and thiamine following thermal processing at three temperatures are shown in Table 1. Each reading represented observation of a single can. Data from four test cans within a given run indicated low standard deviations (0.91 to 2.42) with a coefficient of variation (standard deviation/mean $\times$ 100) of less than 3% indicating good reliability of the technique for centerpoint nutrient evaluation. Because of the small size of the stainless steel sample pans, high thermal conductivity of steel and the use of only a small quantity (75 μL) of liquid sample, the temperature of the liquid in the capsule was assumed to be uniform and identical to the temperature at the center of the can. Since, it was difficult to simultaneously place the sample pan and insert the thermocouple to the central location of the same test can, these were carried out in different cans. A large number of replicates of temperature measurement tests were carried out to get a reliable estimate of heat penetration data for prediction of center time-temperatures.

Heat Penetration Characteristics of Celite

The simulated food model of wetted celite packed in cans at the concentration of 32% celite employed for the studies showed a characteristically unbroken

TABLE 1.
CENTERPOINT NUTRIENT RETENTION IN A THERMO-PROCESSED FOOD MODEL

		Centerpoint Nutrient Retention, %		
		Process Temperature, ^{o}C/(Time, min)		
Sample type	Capsule number	126.7 (30)	121.1 (50)	115.6 (80)
Ascorbic acid	1	95.7	93.1	87.2
	2	97.5	96.0	82.6
	3	95.0	94.3	83.6
	4	97.5	94.1	84.6
	Mean	96.4	92.1	84.5
	SD	1.10	0.62	1.71
	CoV	1.14	0.67	2.03
Thiamine	1	84.2	84.4	79.7
	2	86.6	88.2	84.7
	3	84.9	88.6	78.2
	4	85.8	88.9	81.5
	Mean	85.4	88.8	81.0
	SD	0.91	0.44	2.42
	CoV	1.06	0.49	2.99

SD = Standard deviation; CoV = Coefficient of variation (%)

conduction heating behavior during the heat processing (Fig. 1). The heat penetration characteristics of the celite food model are summarized in Table 2. The f_h values for the test samples of wetted celite in 211 × 400 cans for heating in steam at various retort temperatures ranged from 25.0 to 30.3 min with a standard deviation of 1.56 min. An average thermal diffusivity of 2.06 × 10^{-7} m^2/s was calculated using the relationship, diffusivity = $0.398/[f_h(1/a^2+0.427/L^2]$ where 2L and 2a were the height and diameter of the rest can (Ball and Olson 1957). This value was somewhat higher than the diffusivity range normally associated with common foods (Mohsenin 1980), but was characteristically similar to the value of pureed foods (Mulley *et al.* 1975) and therefore considered to heat at rates comparable to pureed conduction heating foods.

Kinetic Parameters for Ascorbic Acid and Thiamine

The detailed evaluation of kinetic parameters, D and z values, for ascorbic acid and thiamine under various conditions and testing methods are detailed elsewhere (Ghazala and Ramaswamy 1989; Ghazala *et al.* 1989). Kinetic data pertinent to test samples used in this study are summarized in Table 3.

Experimental Versus Predicted Centerpoint Nutrient Retention

The predicted centerpoint nutrient retentions (100 - % destroyed), employing kinetic data, heat penetration parameters and processing conditions, and using

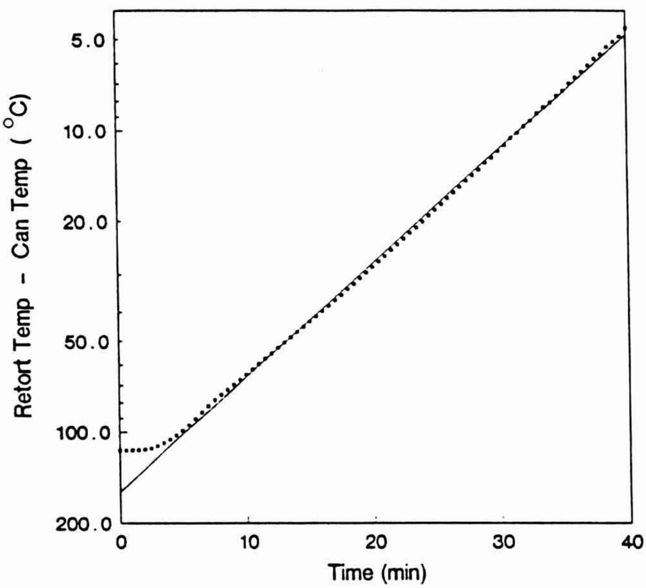

FIG. 1. TYPICAL HEAT PENETRATION CURVE FOR THE FOOD MODEL

TABLE 2.
HEAT PENETRATION PARAMETERS FOR THE CELITE FOOD MODEL

Parameter	Mean[1]	SD	CoV
Heating rate index (f_h), min	26.86	1.60	6.0
Cooling rate index (f_c), min	35.12	1.55	4.4
Heating rate lag factor (j_{ch})	2.22	0.0759	3.5
Cooling rate lag factor (j_{cc})	2.66	0.0688	2.6

[1] based on 96 observations; SD = Standard deviation; CoV = Coefficient of variation (%)

the three models (Ball, Teixeira, and Finnegan) are shown in Table 4. Ball's model was based on the experimental heat penetration parameters, f_h and j_{ch} with the assumption that $f_h = f_c$ and $j_{cc} = 1.41$. Finnegan's modification (Finnegan 1984) is a slight improvement in terms of accommodating the early portion of cooling curve to hyperbolically fit the experimentally determined f_c and j_{cc} values. Teixeira's approach (Teixeira *et al.* 1969) is based on solving the heat transfer equation using finite difference approximation. The input for the program is the f_h value (it also assumes that $f_h = f_c$).

Among the three predictions, Ball's model gave slightly higher retention values perhaps due to its conservative use of lethality contributed in the cooling section, while the other two models accommodate the cooling phase. There were small differences in the retention value predicted by Teixeira's model and Finnegan's model due to differences in the treatment of cooling data. While Finnegan's model made use of the cooling parameters, f_c and j_{cc}, Teixeira's approach was based on $f_h = f_c$ and an instantaneous cool-start. The heat penetration data (Table 2) indicated some differences between f_h and f_c as well as between j_{ch} and j_{cc}.

TABLE 3.
KINETIC PARAMETERS FOR THERMAL DESTRUCTION
OF ASCORBIC ACID AND THIAMINE

Sample	D value (min at 121.1°C)	z value (°C)
Ascorbic acid	600 ± 6.7	32.1
Thiamine	394 ± 8.2	26.4

TABLE 4.
COMPARISON OF EXPERIMENTAL CENTERPOINT RETENTION VALUES WITH PREDICTION FROM VARIOUS MODELS

Particulars	Nutrient Retention, % (deviation, %) Process Temperature, °C 126.7	121.1	115.6
Ascorbic acid			
Experimental	96.4	92.1	84.5
Ball	97.2 (+0.8)	92.1 (0.0)	87.1 (+3.0)
Teixeira	95.9 (-0.5)	92.3 (+0.2)	87.9 (+3.9)
Finnegan	95.8 (-0.7)	90.1 (-2.2)	86.5 (+2.3)
Thiamine			
Experimental	85.4	88.8	81.0
Ball	96.7 (+11.7)	89.5 (+0.8)	83.2 (+2.6)
Teixeira	94.7 (+9.8)	89.7 (+1.0)	84.4 (+4.0)
Finnegan	95.0 (+10.1)	86.8 (-2.2)	82.2 (+1.4)

A comparison of the experimental centerpoint nutrient retention results with the predicted values showed excellent agreement with less than 4% discrepancy between experimental and predicted values in five out of six conditions. The poor agreement between the predicted and experimental values for thiamine at 126.7°C could only be ascribed to an experimental error since there was no other logical explanation.

The predicted values were based on centerpoint temperature-time response while the experimental values are from test capsules placed at the center. The temperature response in a small volume surrounding the centerpoint can generally be assumed to be somewhat similar due to the geometrical symmetry in terms of heat transfer reaching the center. This aspect was further explored theoretically using Teixeira's finite difference program. Considering a 10 × 10 space grid for a can of radius 3.25 cm and 9.52 cm height, the size of the test capsule fits within the space occupied by the adjoining nodes in the radial and longitudinal directions. The temperatures at the center [T(NR, NH)] as well as the two other nodes [T(NR-1, NH), T (NR, NH-1)] were predicted using conditions matching one of the test runs (Table 5). The results indicated that the maximum differences between the three temperatures was 1.0°C up to about 12 min (product temperature during this period was below 60°C) and after 28 min the differences were less than 0.2°C. These results suggested that it was valid to assume that the capsule temperature and center temperature were similar.

TABLE 5.
PREDICTED NODAL TEMPERATURES AT THE CENTER AND TWO ADJOINING NODES (RADIAL AND LONGITUDINAL) USING TEIXEIRA'S PROGRAM

Time (min)	Nodal Temperature (^{o}C)		
	Central T(NR,NH)	Radial T(NR-1,NH)	Longitudinal T(NR,NH-1)
0	15.0	15.0	15.0
2	15.0	15.0	15.0
4	16.3	16.7	16.3
6	22.0	22.7	22.0
8	30.9	31.9	31.1
10	41.2	42.2	41.4
12	51.4	52.4	51.7
14	61.0	61.8	61.3
16	69.5	70.3	69.9
18	77.1	77.7	77.5
20	83.7	84.2	84.0
22	89.4	89.8	89.7
24	94.3	94.6	94.5
26	98.4	98.7	98.7
28	102.0	102.2	102.2
30	105.0	105.2	105.2
32	107.5	107.7	107.7
34	109.7	109.8	109.8
36	111.5	111.6	111.6
38	113.1	113.2	113.2
40	114.4	114.5	114.4
42	115.5	115.5	115.5
44	116.4	116.5	116.4
46	117.2	117.2	117.2
48	117.8	117.9	117.9
50	118.4	118.4	118.4

Retort Temperature, 121.1^{o}C; 10 x 10 spatial matrix, time step, 0.125 min.
(NR, NH): Radial and longitudinal nodal coordinates at the can center.

CONCLUSIONS

A methodology was established for studying the centerpoint nutrient degradation in thermo-processed conduction heating foods. It provides a convenient means of obtaining locational thermal destruction of nutrients in cans undergoing sterilization for verification of computer models. In addition to studying nutrient destruction in still processes, these capsules offer potential as carriers of nutrients or microbial spores in UHT aseptic processes where time-temperature measurements are extremely difficult.

REFERENCES

ADAMS, J. P., PETERSON, W. R. and OTWELL, W. S. 1983. Processing of seafood in institutional-sized pouches. Food Technol. *37*(4), 123.

BALL, C. O. 1923. Thermal process times for canned food. Bull. 37. National Research Council, Washington, DC.

BALL, C. O. and OLSON, F. C. W. 1957. *Sterilization in Food Technology,* McGraw-Hill Book Co., New York.

CASTILLO, P. F., BARREIRO, J. A. and SALAS, G. R. 1980. Prediction of nutrient retention in thermally processed heat conduction food packaged in retortable pouches. J. Food Sci. *45,* 1513.

DOWNES, T. W. and HAYAKAWA, K.-I. 1977. A procedure for estimating retention of components of thermally conductive processed foods. Lebensm.-Wiss. u. Technol. *10,* 256.

FINNEGAN, N. 1984. Development of an intelligent interactive microcomputer software package for the optimization of batch sterilization processes. M.Sc. Thesis, Dept. Agric. Eng., Macdonald College of McGill Univ. Ste Anne de Bellevue, PQ, Canada.

GHAZALA, S. and RAMASWAMY, H. S. 1989. High temperature degradation kinetics of thiamine in aqueous systems. *In Review.* J. Sci. Food and Agriculture.

GHAZALA, S., RAMASWAMY, H. S., VAN DE VOORT, F. R., PRASHER, S. and BARRINGTON, S. 1989. Kinetics of ascorbic acid degradation in aqueous media at high temperatures. *In Review.* J. Food Science.

HERSOM, A. C. and SHORE, D. T. 1981. Aseptic processing of foods comprising sauce and solids. Food Technol. *35*(5), 53.

HOLDSWORTH, S. D. 1985. Optimization of thermal processing—A review. J. Food Proc. Eng. *4,* 89.

HUNTER, G. M. 1972. Continuous sterilization of liquid media containing suspended particles. Food Technol. Australia, *24*(4), 158.

JEN, Y. Y., MANSON, J. E., STUMBO, C. R. and ZAHRADNIK, J. W. 1971. A simple method for estimating sterilization and nutrient and organoleptic factor degradation in thermally processed foods. J. Food Sci. *36,* 692.

LENZ, M. K. and LUND, I. B. 1980. Experimental procedures for determining destruction kinetics of food components. Food Technol. *34*(2), 51.

MANJI, B. and VAN DE VOORT, F. R. 1985. Comparison of two models for process holding time calculations: Convection system. J. Food Protection, *48,* 359.

MANSON, J. E., STUMBO, C. R. and ZAHRADNIK, J. W. 1970. Evaluation of lethality and nutrient retentions of conduction heating foods in rectangular containers. Food Technol. *24*(11), 109.

MOHSENIN, N. N. 1980. *Thermal Properties of Foods and Agricultural Materials,* Gordon and Breach Sci. Publ., New York.

MULLEY, E. A., STUMBO, C. R. and HUNTING, W. M. 1975. Kinetics of thiamine degradation by heat. A new method for studying reaction rates in model systems and food products at high temperatures. J. Food Sci. *40,* 985.

OHLSSON, T. 1980. Optimal sterilization temperatures for sensory quality in cylindrical containers. J. Food Sci. *45,* 1517.

PFLUG, I. J., SMITH G., HALCOMB, R. and BLANCHETT, R. 1980a. Measuring sterilizing values in containers of food using thermocouples and biological indicator units. J. Food Protection, *45,* 940.

PFLUG, I. J., JONES, A. T. and BLANCHETT, R. 1980b. Performance of bacterial spores in a carrier system in measuring the Fo-value delivered to cans of food heated in a Steritort. J. Food Sci. *45,* 119.

RODRIGUEZ, A. C. and TEIXEIRA, A. A. 1988. Heat transfer in hollow cylindrical rods used as bioindicator units for thermal process validation. Trans. Amer. Soc. Agri. Eng. *31*(4), 1233.

TEIXEIRA, A. A., STUMBO, C. A. and ZAHRADNIK, J. W. 1975. Experimental evaluation of mathematical and computer models for thermal process evaluation. J. Food Sci. *40,* 653.

TEIXEIRA, A. A., DIXON, J. R., ZAHRADNIK, J. W. and ZINSMEISTER, G. E. 1969. Computer optimization of nutrient retention in the thermal processing of conduction-heated foods. Food Technol. *23,* 848.

THIJSSEN, H. A. C. and KOCHEN, L. H. 1980. Calculation of optimum sterilization conditions for packed conduction-type foods. J. Food Sci. *45,* 1267.

YAMANO, Y. 1976. Studies on thermal processing of flexible food packages by steam-and-air retort. Ph.D. Thesis, Kyoto University, Kyoto, Japan.

SIMULATION OF CANOLA AND BARLEY DRYING IN A DEEP BED

STEFAN CENKOWSKI, WILLIAM E. MUIR and DIGVIR S. JAYAS

Department of Agricultural Engineering
University of Manitoba
Winnipeg, Canada, R3T 2N2

Accepted for Publication October 18, 1989

ABSTRACT

A mathematical model for a radial, continuous-crossflow dryer was modified and used to simulate the drying process in a fixed bed dryer. The predictions of the adapted model were compared with experimental test results for canola drying at the following drying conditions: airflow rates of 0.4 and 0.6 kg/(m^{2}s), inlet air humidity 0.098 and 0.0114 kg/kg of dry air, initial grain moisture content 0.221 and 0.251 kg/kg dry basis. In both tests the inlet drying air temperature was kept at an average of 67.5°C. At the end of canola drying, the mean drying air temperature predicted by our model was within 1°C of the measured temperature and the mean predicted moisture content was within 0.5% of the measured moisture content, dry basis. Also, our model was verified against experimental results for barley published by other authors and against predictions from a published model for barley. The predictions from our model were in good agreement with the published experimental and predicted data. Simulations results for canola and barley drying in the same thickness of a deep bed were compared. Simulations were conducted to investigate the effects of canola properties such as bulk density and drying conditions of air such as airflow rate and air humidity on drying in deep beds of canola.

INTRODUCTION

Mathematical modelling and computer simulation of drying of agricultural products are now widely used in research to predict and compare performance of different drying systems and match them with the crop quality after drying. Many different models have been proposed to describe the drying process in the basic types of convective grain dryers (O'Callaghan *et al.* 1971; Bakker-Arkema *et al.* 1974; Ingram 1976; Bruce 1984; Cenkowski and Sokhansanj 1988). The

Journal of Food Process Engineering **12** (1990) 171–190. *All Rights Reserved.*

accuracy of predictions from these models is highly dependent on the completeness of the mathematical description of the drying phenomena and empirical relationships used to describe drying and rewetting characteristics of grain. Mathematical descriptions are being made more precise but still the main limitation in accuracy of the predicted results from these models is due to the limitations of the introduced empirical expressions. Some of these models are general enough to simulate drying in different types of dryers and drying of different crops. One can still expect, however, significant discrepancies between computed and experimental results when the mathematical model has not been tested for a specific crop.

At present, little is known about the drying behavior of canola seed. The usual practice of drying canola in the swath over a 5–12 day period causes high shattering losses. Canola destined for long-term storage should be at 8% moisture content (wet basis) or less (Otten *et al.* 1989). Canola can be combined at a moisture content of 15% and then dried prior to storage. But to introduce such a practice for canola many different aspects should be considered among them the drying behavior of canola in a deep bed. One of the ways to do this is by using a computer simulation.

The primary objective of the paper was to adapt the crossflow model of Cenkowski and Sokhansanj (1988) to a deep bed drying process and to verify the mathematical model against experimental data obtained by Cenkowski during drying of canola. The second objective was to verify the adapted model against the experimental data of Boyce for drying barley in a fixed bed (experimental data of Boyce were taken from Ingram 1976 and O'Callaghan 1971). The third objective was to compare the predicted results of our adapted crossflow model against those from the Ingram (1976) model. Finally, the last objective was to compare the drying processes of canola and barley in deep beds by using the simulation model and to investigate the effects of grain parameters and drying conditions on canola drying.

THEORETICAL DEVELOPMENT

In a fixed bed dryer, the grain bed is stationary and drying proceeds with time. In a moving bed crossflow dryer, the grain bed dries as it moves downward. Drying time (θ) in a fixed bed is equivalent to the time taken for the bed of grain to move a distance of y in a crossflow dryer ($\theta = y/v_g$, where v_g is the grain velocity). Based on this similarity, we used the crossflow model of Cenkowski and Sokhansanj (1988) to simulate drying in a fixed bed dryer.

If a circular control volume is cut off and straightened out then one can obtain a typical thin layer (Fig. 1). After transformation from a circular control volume to a thin layer the equations presented by Cenkowski and Sokhansanj (1988) have the following form:

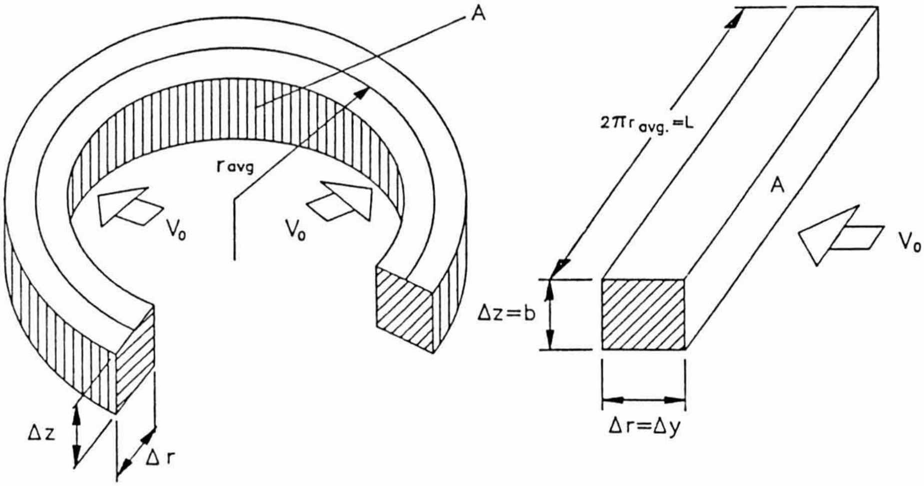

FIG. 1. TRANSFORMATION FROM CIRCULAR CONTROL VOLUME TO A THIN LAYER

For air temperature (for layer i after time θ)

$$t_{ai,\theta} = t_{a(i-1),\theta} - \frac{t_{a(i-1),\theta} - t_{gi,(\theta-1)}}{A\ v_0\ c_{ai,\theta}\ m_{i,\theta}} \{ 1 - \exp[-h_{vi,\theta}\ \Delta y\ A\ m_{i,\theta}]\} \tag{1}$$

where:

$$m_{i,\theta} = \frac{1}{A\ v_0\ \rho_{ai,\theta}\ c_{ai,\theta}} - \psi_{i,\theta} \frac{\Delta\theta}{G_{i,\theta}\ c_{gi,\theta}} \tag{2}$$

sensible heat ratio $\psi_{i,\theta}$:

$$\psi_{i,\theta} = \frac{\Delta q_{s(i,\theta)}}{\Delta q_{s(i,\theta)} + \Delta q_{l(i,\theta)}} = \frac{G_{i,\theta}\ c_{gi,\theta}\ [t_{si,\theta} - t_{g(\theta-1),i}]}{G_{i,\theta}\ c_{gi,\theta}\ [t_{si,\theta} - t_{g(\theta-1),i}] + G_d\ \Delta M_{i,\theta}\ h^*_{fg}} \tag{3}$$

The temperature of a spherical body can be described by a lump model provided that the Biot Number, Bi, is less than 0.1; and can be expressed throughout the drying chamber as follows:

$$t_{si,\theta} = t_{a(i-1),\theta} - [t_{a(i-1),\theta} - t_{gi,(\theta-1)}] \exp\{- \frac{6\ h_{i,\theta}\ \Delta\theta}{c_{gi,\theta}\ \rho_{gi,\theta}\ d_{i,\theta}}\} \tag{4}$$

Enthalpy Change of Grain

Each layer of grain during the step $\Delta\theta$ loses heat by evaporation, but also gains heat by convective heat transfer. The difference in enthalpy of the air, $\Delta h_{a_{i,\theta}}$, and the heat used for moisutre evaporation from the grain, $\Delta q_{l_{i,\theta}}$, is equal to the change in the sensible heat of grain, $\Delta q_{s_{i,\theta}}$ during the time step:

$$\Delta h_{a_{i,\theta}} - \Delta q_{l_{i,\theta}} = \Delta q_{s_{i,\theta}} \tag{5}$$

where:

$$\left.\begin{aligned}
\Delta h_{a_{i,\theta}} &= h_{a_{i,\theta}}(in) - h_{a_{i,\theta}}(out) \\
h_{a_{i,\theta}}(in) &= c_{ad}\, t_{a(i-1),\theta} + H_{(i-1),\theta}\,(2500 + c_{av}\, t_{a(i-1),\theta}) \\
h_{a_{i,\theta}}(out) &= c_{ad}\, t_{a_{i,\theta}} + H_{i,\theta}\,(2500 + c_{av}\, t_{a_{i,\theta}}) \\
\Delta q_{l_{i,\theta}} &= \Delta M_{i,\theta}\, G_d\, h^{*}_{fg_{i,\theta}} \\
\Delta q_{s_{i,\theta}} &= G_{i,\theta}\, c_{g_{i,\theta}}\,(t_{g_{i,\theta}} - t_{g_{i,(\theta-1)}})
\end{aligned}\right\} \tag{6}$$

Latent heat of vaporization of water from moist grain $h^*_{fg_{i,\theta}}$ is dependent on temperature and moisture content. Based on the Clyperon equation, Othmer (1940) and Gallaher (1951) established the following formula for the h^*_{fg} in agricultural crops:

$$h^*_{fg} = h_{fg}\,[1 + a \exp(b\, M)] \tag{7}$$

with temperature dependency provided by the latent heat of vaporization of free water h_{fg}.

The temperature of the thin layer, i, at time, θ, is calculated from the enthalpy change of grain

$$t_{gi\theta} = \frac{\Delta h_{a_{i,\theta}} - \Delta q_{l_{i,\theta}}}{c_{g_{i\theta}}\, G_{i\theta}} + t_{g_{i,(\theta-1)}} \tag{8}$$

Deep Bed Drying Simulation

The general procedure of calculation is similar to that given by Boyce (1965), Thompson *et al.* (1968), or O'Callaghan *et al.* (1971). The deep bed of grain is divided into a number of thin layers that are sufficiently thin for the application of the thin layer equations. The temperatures and moisture contents of air and grain are calculated layer by layer with a sufficiently short step time, $\Delta\theta$. There is one limitation imposed on the calculation procedure: that is the maximum value of relative humidity, RH, of the air passing through the set of the thin layers. This value is limited to 0.8 (Eq. 8). The RH limit was set for two reasons: (1) equilibrium moisture content (EMC) equations have a good agreement with experimental data up to 0.8 RH, beyond this point the equations usually underpredict the EMC (Cenkowski *et al.* 1989) and (2) some authors (Boyce 1965; Ingram 1976) confirmed that there is a tendency for computed moisture content in the upper layer of the bed to be less than observed. It might be also attributable to errors in determining the constants in the thin layer equations which have a cumulative effect. That is why, when the relative humidity exceeds 80%, the partial pressure of water vapour at saturation, P_{vs}, is calculated as follows:

$$P_{vs_{i,\theta}} = \frac{H_{i,\theta}\ P_{AT}}{0.80\ (0.622 + H_{i,\theta})} \tag{9}$$

and then again the air temperature, $t_{a_{i,\theta}}$, is recalculated according to the empirical equation for calculation of values of temperature at saturation given by Chau (1980):

$$t_{a_{i,\theta}} = 34.20975\ P_{vs_{i,\theta}}^{\ 0.2203603} + 7.048104\ \log(P_{vs_{i,\theta}}) - 27.226 \tag{10}$$

The model is sensitive to parameters introduced into the empirical equations which have been used in the model. For drying air temperatures 2–5°C above the grain temperature, the calculated changes in enthalpy of the drying air passing across the layers might become negative because some coefficients used in the model (for example the heat transfer coefficient) may be in error. In this case the calculation procedure is changed to a heat and mass balance procedure. There are two cases considered here:

(1) If in the calculations, the enthalpy change of the air across the layer is negative then the thin layer equation is replaced and changes in grain moisture are calculated assuming that the enthalpy of the air entering the layer equals the enthalpy of the air leaving the layer of grain. From an enthalpy balance the new air humidity is calculated as follows:

$$H_{i,\theta} = \frac{h_{a_{i,\theta}}(in) - c_{ad}\ t_{a_{i,\theta}}}{2500 + c_{av}\ t_{a_{i,\theta}}} \tag{11}$$

and the change in moisture content of the layer is:

$$\Delta M_{i,\theta} = \frac{[H_{i,\theta} - H_{i,(\theta-1)}]\ A\ v_0\ \rho_{i,\theta}\ \Delta\theta}{G_{d_{i,\theta}}} \tag{12}$$

(2) If in the calculations, the change in enthalpy of the air, $\Delta h_{a_{i,\theta}}$, during the time step, $\Delta\theta$, is less than the change in the latent heat of the grain and the change in the air enthalpy, $\Delta h_{a_{i,\theta}}$, is positive then again the thin layer equation is replaced by the heat balance equation that:

$$\Delta h_{a_{i,\theta}} = \Delta q_{l_{i,\theta}} \tag{13}$$

and the change in grain moisture content is calculated by:

$$\Delta M_{i,\theta} = \frac{\Delta h_{a_{i,\theta}}}{G_d\, h^*_{fg_{i,\theta}}} \tag{14}$$

Empirical Drying Equations and EMC Equations

The drying of canola and barley was assumed to be described by the following equation (O'Callaghan *et al.* 1971; Sokhansanj *et al.* 1984):

$$\frac{dM}{d\theta} = -\, k\, [M(\theta) - M_e] \tag{15}$$

The drying constant, k, for canola in the temperature range 20°C $\leqslant t_a \leqslant$ 70°C was described (unpublished data and data from Singh *et al.* 1983; Sokhansanj *et al.* 1984) by the following coefficients at different moisture content ranges:

$$\left.\begin{array}{ll} k = 0.0012\, t_a - 0.017 & \text{when } 0.25 \text{ db} \geq M \geq 0.10 \text{ db}, \\ k = 0.0004\, t_a & \text{when } 0.10 \text{ db} > M \geq 0.04 \text{ db}, \\ k = 0.0002\, t_a & \text{when } M \leq 0.04 \text{ db}. \end{array}\right\} \tag{16}$$

The equilibrium moisture content M_e was calculated according to the modified Henderson equation and the constants given by Sokhansanj *et al.* (1986):

$$RH = 1 - \exp[-B\, (t_a + C)\, (100\, M_e)^n] \tag{17}$$

The values of the constants were: B = 0.0005056, C = 40.1204, n = 1.5702.

The constant, k, for barley in the equation was taken as follows (O'Callaghan *et al.* 1971):

$$k = 139.3 \exp\{\frac{-4426}{t_a + 273}\}. \tag{18}$$

A dynamic equilibrium moisture content expression for barley was taken to be that suggested by Ingram (1976):

$$M_e = 0.2163 - 0.0357 \ln(t_a) - 0.0673 \ln(1 - RH) \tag{19}$$

Latent Heat of Vaporization

Generally it is thought that above 12% moisture content db there is little difference between the heat of vaporization of grain h^*_{fg} and that of free water h_{fg} (Othmer 1940; Gallaher 1951; Boyce 1965). A study of equilibrium moisture data for different cereals indicates that the latent heat of vaporization of grain moisture would be similar for kernels of approximately the same dimensions (Boyce 1965). The parameters $a = 23$ and $b = -40$ in Eq. 7 were used for barley drying simulations in the papers from Boyce (1965) and Ingram (1976).

There are no published data available on latent heat of vaporization for moist canola. The equilibrium moisture content data for rapeseed published by Pichler 1957 were used to establish the latent heat of canola. From equilibrium moisture content curves the equilibrium relative humidity was read at various temperatures and moisture contents. By plotting partial vapor pressure against saturated vapor pressure at the same temperature for each moisture content, the ratios h^*_{fg}/h_{fg} were determined. (This method has been used for other crops and explained in detail by Gallaher 1951; Sutherland *et al.* 1971; Bala and Woods 1984.) The curve drawn through the points of h^*_{fg}/h_{fg} vs moisture content for rapeseed by the method of least squares is described by Eq. 7 with the following parameters: $a = 4.7$, $b = -44.2$ for $M \leqslant 0.075$ db and $a = 0.5$, $b = -14.5$ for $M > 0.075$ db.

Physical and Thermal Properties

The dry-basis bulk densities of canola and barley were taken as 680 kg/m^3, (Jayas *et al.* 1989) and 490 kg/m^3 (O'Callaghan *et al.* 1971, run B134), respectively.

The specific heat of canola and barley were calculated using the following equations:

$$\begin{aligned} &\text{Canola} \quad C_g = 1.3953 + 2.05\,M \quad \text{(Sharma and Muir 1973)} \\ &\text{Barley} \quad C_g = 1.3 + 4.19\,M \quad \text{(O'Callaghan } et\ al. \text{ 1971)} \end{aligned} \tag{20}$$

Average surface heat transfer coefficient for canola, h, for layer i and time θ was calculated from the Nusselt number:

$$h = \frac{Nu\ \lambda}{d} . \tag{21}$$

Gorbis (1964) reported the expression for Nusselt number for a small sphere:

$$Nu = 0.143\ Re^{0.67} \qquad 10 \leq Re \leq 161000 \tag{22}$$

where:

$$Re = v\ d/\nu$$

Finally, volumetric heat transfer coefficient for canola was calculated assuming the canola kernels as spheres (Pabis 1982):

$$h_v = \frac{6\ (1 - \varepsilon)\ h}{d} \tag{23}$$

The volumetric heat transfer coefficient for barley was taken from O'Callaghan *et al.* 1971:

$$h_v = 856.8 \left(\frac{v_0\ \rho_a\ (t_a + 273)}{P_{AT}} \right)^{0.6011} \tag{24}$$

EXPERIMENTAL PROCEDURE

The experimental apparatus comprises three main components: the drying chamber, the heating system together with the ventilator, and the data collecting system (Fig. 2).

The drying chamber is well insulated and consists of a double wall with a space between the walls of 1.5 cm. The walls are made of a 0.5 cm thick paperboard. The drying chamber consists of two deep beds with fixed floors (7a and 7b in Fig. 2) and three removable trays (8a, 8b, 8c). One tray is located at the bottom of the chamber (8a), a second tray is located in the middle of the chamber (8b), 33 cm above the first tray. The third one (8c) is at the top of the drying chamber, 33 cm above the second removable tray. Each tray can hold a 1-cm thick layer of grain.

Copper-constantan thermocouples were placed at five levels (Fig. 2). At each level three thermocouples, placed at different horizontal positions, recorded air temperature. The thermocouples were connected to a datalogger whose output

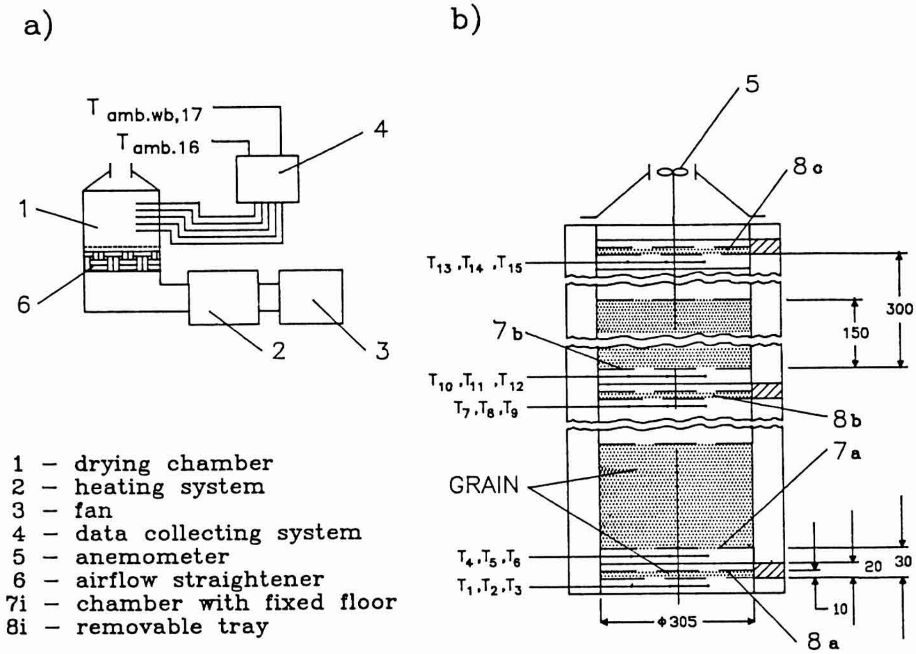

FIG. 2. FIXED BED EXPERIMENTAL DRYER (a) OVERALL SCHEMATIC, (b) DETAIL OF THE DRYING CHAMBER

was recorded every 2 min. The airflow was measured using a turbine anemometer in a cone (Fig. 2).

Prior to each drying experiment, the two chambers with the fixed floors (7a, 7b) were filled to a depth of only 15 cm each with moist canola (*Brassica campestris,* cv. Tobin), tempered before the tests at 20°C for at least 4 h (Sokhansanj *et al.* 1983). The two upper thin-layer trays (8b, 8c) were filled with 1-cm layers of canola. The bottom tray (8a) was removed and a special cover, made of styrofoam, was placed through the opening under the floor of the fixed bed to protect the oilseeds against drying before the drying test was started. The fan was started and the drying air was passed through the opening at the bottom of the chamber. The inlet air temperature to the dryer fluctuated within ± 1°C over time. When thermocouples 1, 2, 3 indicated the desired inlet air temperature, the fan was stopped for about 30 s. The styrofoam cover was removed and the tray (8a) with a 1-cm layer of canola was placed in the opening and sealed with a rubber ring. The fan was started again and simultaneously a computer program for collecting data was initiated. The masses of the removable trays were taken every 10 to 20 min. The time needed to take the mass of the three trays was between 50 to 60 s and during this time the fan was stopped. At the end of drying, two 30-g canola samples from each tray were taken for final moisture content determination by drying samples at 130°C for 4 h in a convection oven (ASAE 1987).

Six tests were performed by drying canola at initial moisture contents ranging from 0.19 to 0.26 db, airflow rates from 0.15 to 0.61 kg/(m^{2}s), relative humidities of the ambient air from 40 to 64% and for two different total thicknesses of drying beds: 33 and 53 cm. Drying air temperature at the inlet to the drying chamber was kept constant at 67.5°C. Two typical tests from these experiments were selected to compare the simulation results.

VALIDATION OF THE SIMULATIONS

Our model was tested by comparing the predicted results with experimental data for canola drying. The input data used in the simulations and experiments are given in Table 1.

Simulated and measured temperatures for drying canola in a fixed bed agreed reasonably well at two significantly different airflow rates 0.4 and 0.6 kg/(m^{2}s) (Fig. 3 and 4). The discrepancies between measured and calculated values were less than 1°C at the end of the drying process. Because of the experimental procedure, the inlet air temperature dropped significantly at the beginning of drying and approached the required value after about 10 min. The measured inlet air temperature was used in the simulations as the inlet air conditions under the first layer. Although the measured inlet temperatures are shown as a smooth (dashed) line in Fig. 3 and 4, the temperatures fluctuated about ± 1°C.

The moisture contents of canola at three locations in the experimental dryer are averages for the 1-cm thick layers (Fig. 5 and 6). The locations shown for the data points and predicted lines in these figures are from the bottom of the drying chamber to the beginnings of the 1-cm thick layers. Using the drying coefficient, in the lumped newtonian equation, that depends on moisture and

TABLE 1.
DATA FOR THE SIMULATION

			Boyce run 134	Canola run A	Canola run B
Drying air temperature	t_{a0}	[°C]	68.3	67.5	67.5
Inlet air humidity	H_0	[kg/kg da]	0.006	0.0114	0.0098
Air flow rate	Q_a	[kg/(m^{2}s)]	0.1778	0.40	0.61
Grain initial temp.	t_{g0}	[°C]	21	22.5	24.0
Grain moisture cont.	M_0	[kg/kg db]	0.342	0.251	0.221
Grain bulk density	ρ_b	[kg/m^3]	490	680	680
Grain porosity	ε	[-]	0.46	0.40	0.40
Grain equivalent diameter	d	[m]	0.0032	0.0015	0.0015
Layer thickness	Δy	[m]	0.005	0.005	0.005
Time increment	$\Delta\theta$	[s]	30	6	6

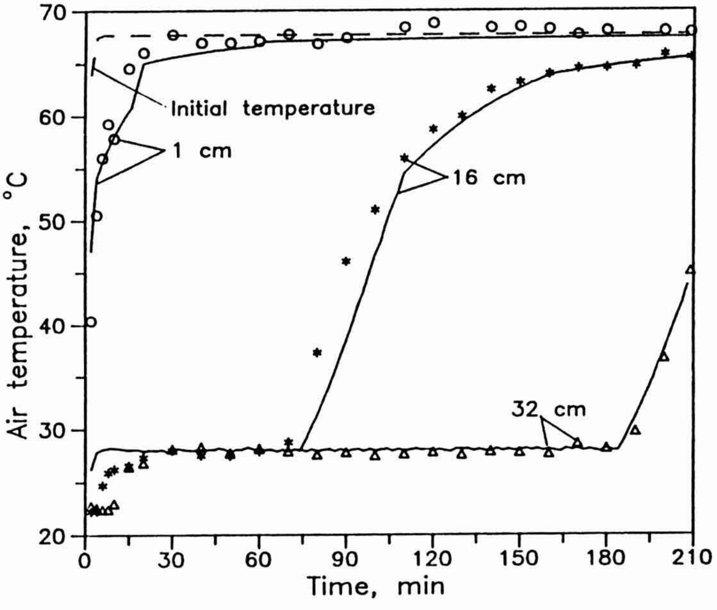

FIG. 3. EXPERIMENTAL (o, *, △) AND SIMULATED (————)
AIR TEMPERATURES AT THREE HEIGHTS ABOVE THE BOTTOM OF
THE DRYING CHAMBER DURING CANOLA DRYING IN RUN A
Initial parameters: Q_a = 0.40 kg/(m^{2}s); M_o = 0.251 kg/kg db.; H_o = 0.0114 kg/kg da.

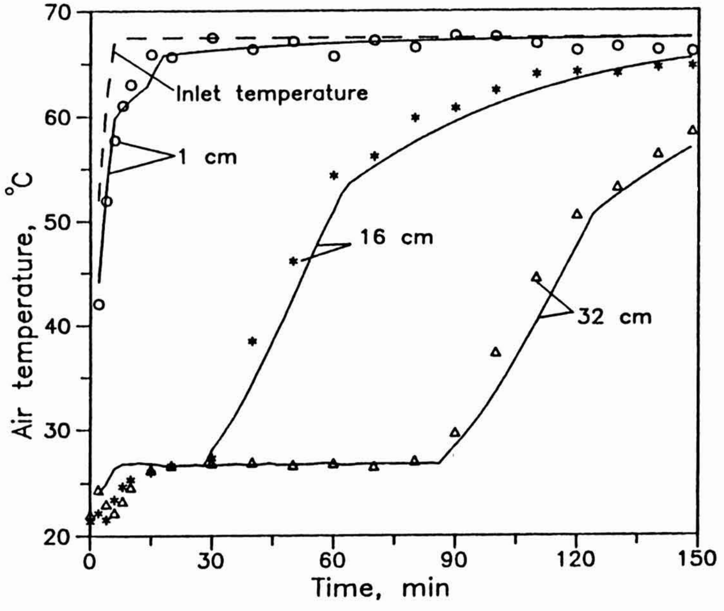

FIG. 4. EXPERIMENTAL (o, *, △) AND SIMULATED (————)
AIR TEMPERATURES AT THREE HEIGHTS ABOVE THE BOTTOM OF
THE DRYING CHAMBER DURING CANOLA DRYING IN RUN B
Initial parameters: Q_a = 0.61 kg/(m^{2}s); M_o = 0.221 kg/kg db.; H_o = 0.098 kg/kg da.

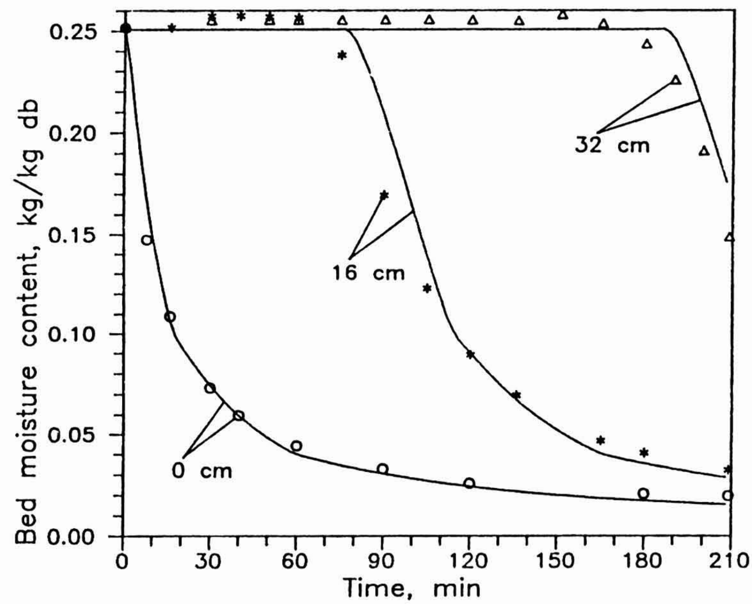

FIG. 5. EXPERIMENTAL (o, *, △) AND SIMULATED (________) CANOLA MOISTURE CONTENTS OF THREE HEIGHTS ABOVE THE BOTTOM OF THE DRYING CHAMBER IN RUN A

Initial parameters: Q_a = 0.40 kg/(m^{2}s); M_o = 0.251 kg/kg db.; H_o = 0.0114 kg/kg da.

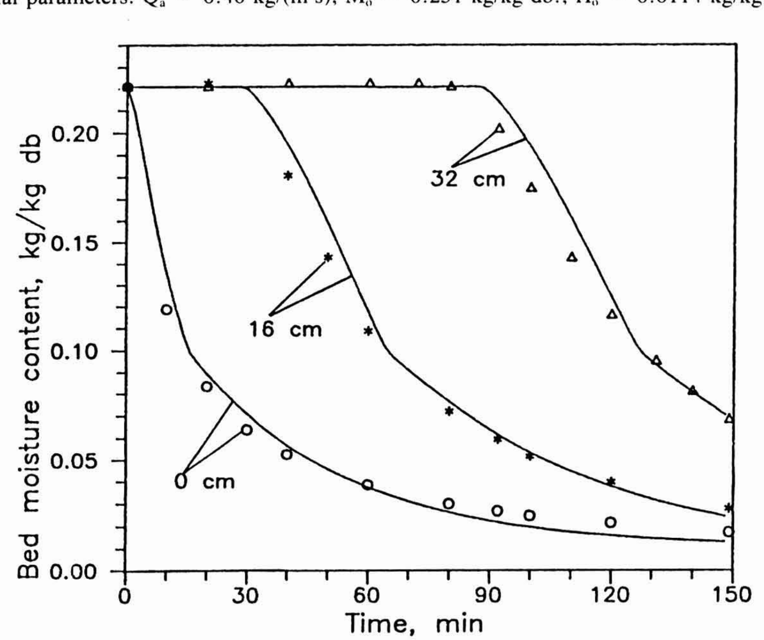

FIG. 6. EXPERIMENTAL (o, *, △) AND SIMULATED (________) CANOLA MOISTURE CONTENTS AT THREE HEIGHTS ABOVE THE BOTTOM OF THE DRYING CHAMBER IN RUN B

Initial parameters: Q_a = 0.61 kg/(m^{2}s); M_o = 0.221 kg/kg db.; H_o = 0.098 kg/kg da.

temperature provided good agreement with the experimental results. The differences between the measured and the simulated moisture contents of canola were less than 0.5% moisture content db.

There were still large differences in moisture content of canola between the bottom and top layers at the end of drying. This was evident from the simulation results as well as from the experiments. Increasing the velocity by 30% in Run B compared with Run A, the difference in moisture content between the bottom and top layers decreased from 0.13 to 0.05 kg/kg db. But in both cases the bottom layer was unacceptably overdried ($\approx$ 0.02 kg/kg db) in our experiment. Assuming that the bottom layer should not be dried below 0.087 kg/kg db ($\equiv$ 8% wb) the required drying time was about 20 min. After the air passed through 16 and 32 cm of canola the required drying time was about 70 and 130 min, respectively in Run B.

Our model was also tested by comparing our predicted results with experimental data of barley drying and with the simulation results of Ingram (1976). Simulations were made of a barley drying experiment carried out by Boyce, the results of which were presented and used by Ingram (1976) and O'Callaghan *et al.* (1971) to verify their models. The input data used in the simulations are given in Table 1.

The model of Ingram (1976) gives good agreement between measured and simulated temperature curves (Fig. 7). The accuracy of that model was improved

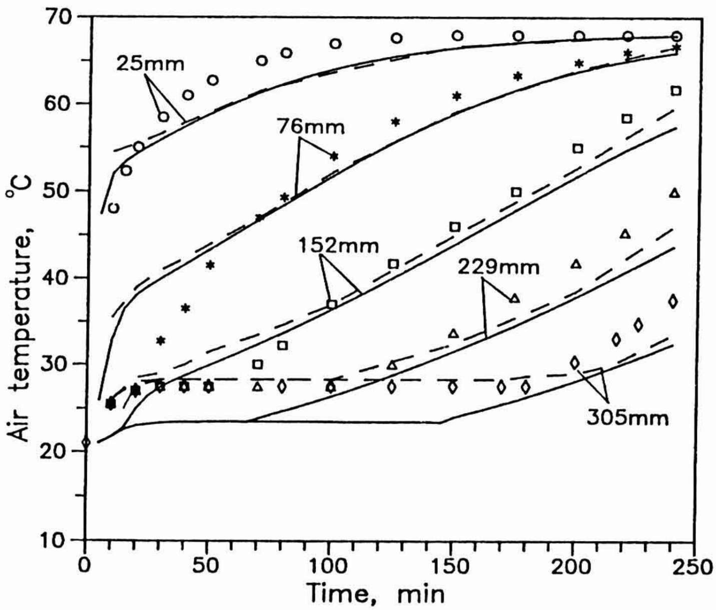

FIG. 7. COMPARISONS FOR DRYING BARLEY OF PREDICTED TEMPERATURES; OUR MODEL (————), INGRAM (1976) MODEL (– – –) AND BOYCE'S MEASURED TEMPERATURES (o, *, □, △, ◇)

by assuming slab geometry for barley. In our model barley was assumed to have a spherical shape. This assumption slightly lowered the calculated air temperatures compared with experimental results (Ingram 1976).

The calculated drying air temperature at which air approached 80% predicted relative humidity was about 23.5°C (305 mm line in Fig. 7) and for that layer the predicted temperatures are about 4°C below the experimental ones. The reason for that might be that the temperature governing the rate of drying is the grain temperature (Boyce 1965; Pabis and Henderson 1962; Sokhansanj *et al.* 1987) and we used the lumped newtonian model as the thin-layer drying equation. For the similar range of drying times the agreement of experimental data with calculated results given by Ingram (1976) for the same top layer is better than ours and the difference is about 1°C above the experimental values. But at the end of drying, the final temperature calculated by Ingram (1976) for that layer is about 4°C lower than the experimental value, which agrees with our predicted result (Fig. 7).

Our predicted moisture content profile through the bed of barley, 160 min after the start of drying, was compared with the measured profile of Boyce and the simulated profile of Ingram (1976) (Fig. 8). Agreement between calculated and observed profiles were reasonably good. Our calculated results were closer

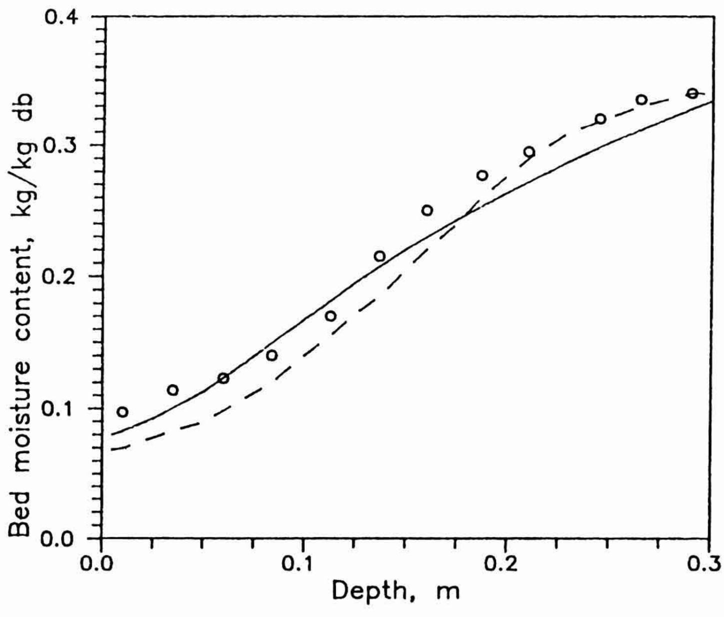

FIG. 8. PREDICTED MOISTURE CONTENT PROFILE THROUGH THE BED AT 160 MIN OF DRYING

Our model (________), Ingram (1976) model (– – –), and experimental values of Boyce (o) to the experimental values than were Ingram's up to 0.15 m of the layer depth. After that simulation results of our model were lower by about 0.002 moisture content in kg/(kg db) compared with the experimental and Ingram's calculated results.

The simulated moisture contents of canola at two locations were compared with similarly located layers for barley (Fig. 9). In calculations it was assumed that the drying air parameters and initial moisture content of canola and barley are the same as in Run A (Table 1). The bulk density of barley was taken from Pabis (1982) as 600 kg/m^3. The layers were 16 cm apart from each other. The small diameter of canola seeds ($\approx$1.5 mm) compared with an equivalent diameter of barley ($\approx$3.2 mm) creates a larger surface area per unit mass that absorbs heat faster. Because of that, for the same drying conditions the drying zone in canola drying is narrow compared with the drying zone for barley and moves faster (Fig. 9).

The effects of drying conditions on canola drying were determined for two layers, each 0.5 cm thick located 0.5 cm and 9.5 cm from the dryer's false floor (Fig. 10 and Table 2). The effect of the air flow rate is represented by simulations S1 and S2. Change in air flow rate from 0.2 to 0.4 kg/(m^{2}s) increased the velocity of the drying front. In simulation test S1 the top layer, dried at the airflow rate

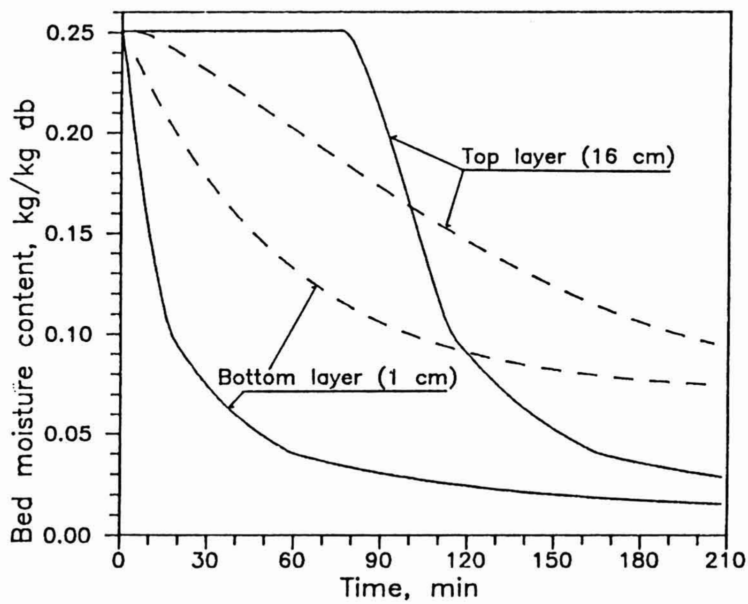

FIG. 9. SIMULATED BARLEY (– – –) AND CANOLA (————) MOISTURE CONTENTS AT TWO HEIGHTS ABOVE THE BOTTOM OF THE DRYING CHAMBER
Initial parameters: t_{ao} = 67.5°C, H_o = 0.0114 kg/kg da, Q_a = 0.40 kg/(m^{2}s); M_o = 0.251 kg/kg db.

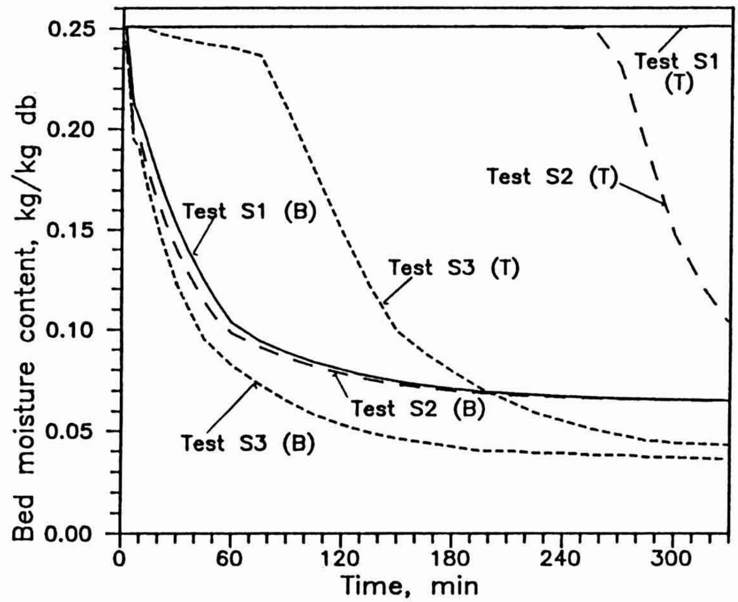

FIG. 10. THE EFFECT OF DRYING PARAMETERS ON CANOLA DRYING IN A 10 CM DEEP BED FOR THE BOTTOM (B) AND TOP (T) LAYERS EACH 5MM THICK
Drying parameters are given in Table 2.

of 0.2 kg/(m^2s), was still at the initial moisture content after 5.5 h of drying, whereas in simulation test S2 by doubling the airflow rate the same top layer dried to about 11% db after the same time of drying.

By decreasing the inlet air humidity the drying zone velocity increases, but simultaneously the equilibrium moisture content of the bottom layer becomes very low which causes overdrying (Fig. 10). These simulations indicate that the

TABLE 2.
DATA FOR CANOLA DRYING SIMULATION

			SIMULATION TESTS			
			S1	S2	S3	S4
Drying air temperature	t_∞	[°C]	40.0	40.0	40.0	40.0
Inlet air humidity	H_0	[kg/kg da]	0.025	0.025	0.0114	0.0114
Air flow rate	Q_a	[kg/(m^2s)]	0.20	0.40	0.40	0.40
Grain initial temp.	t_{g0}	[°C]	22.5	22.5	22.5	22.5
Grain moisture cont.	M_0	[kg/kg db]	0.251	0.251	0.251	0.251
Grain bulk density	ρ_b	[kg/m^3]	680	680	680	760
Grain porosity	ε	[-]	0.40	0.40	0.40	0.34
Grain equivalent diameter	d	[m]	0.0015	0.0015	0.0015	0.0015
Layer thickness	Δy	[m]	0.005	0.005	0.005	0.005
Time increment	$\Delta\theta$	[s]	9	9	9	9

relative humidity of the air entering the dryer should be high (about 60–70%) assuming that the drying air temperature does not exceed 40°C. The dryer should work in a recirculation mode. Only a small portion of fresh, ambient air should be introduced to such a system. This solution could significantly reduce energy consumption. The simulation results indicate the need for further research including investigations of the effects of drying at high relative humidities on canola quality (mould growth).

Bulk density and porosity of a product are important considerations in operating and predicting drying times of canola. Bulk density is affected by many factors such as seed moisture content, the amount and size distribution of foreign material and method used to fill the dryer. The American Society of Agricultural Engineers Data D241.3 (ASAE 1987) gives two values, 644 and 772 kg/m^3, for bulk density of canola. Jayas *et al.* 1989 concluded that for dense fill the bulk density of canola, on average was 11.7% greater and the porosity was 14.2% lower than these properties for loose fill. Based on the above information, the bulk density and porosity were set at 760 kg/(m^3) and 0.34, respectively in the simulation (Test S4, Fig. 11). For the layer located 15.5 cm above the bottom layer an increase in bulk density causes a decrease in drying.

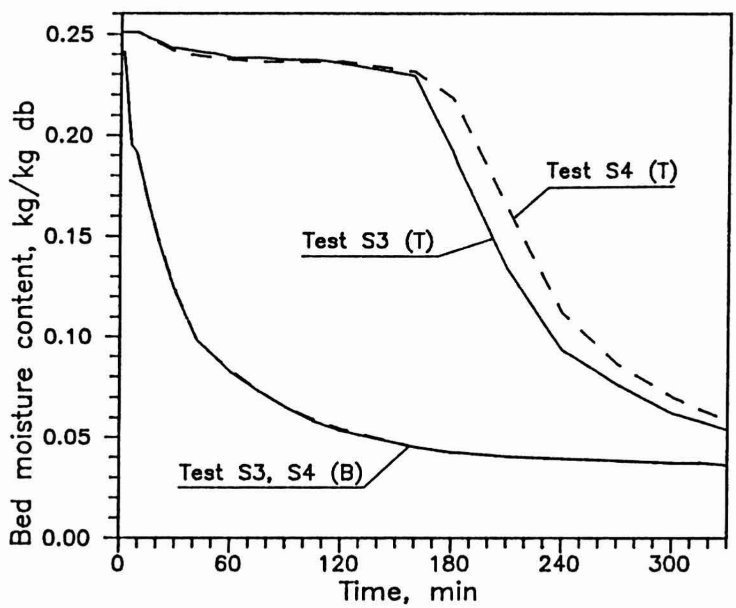

FIG. 11. THE EFFECT OF BULK DENSITY ON CANOLA DRYING IN A 16 CM DEEP BED FOR THE BOTTOM (B) AND TOP (T) LAYERS EACH 5 MM THICK
The drying parameters are given in Table 2.

CONCLUSIONS

Canola drying in a deep bed was simulated by adapting and modifying equations describing crossflow drying. Simulated air temperatures and moisture contents of barley and canola were compared with experimental results published by other authors, predicted by a published model, and our own experimental data obtained during canola drying. The mean difference between predicted and measured drying air temperatures during canola drying was 1°C at the end of drying, and the mean difference for moisture content was less than 0.5% moisture content db. The simulation model was used to investigate the effect of canola density and drying conditions on canola drying in a deep bed. The numerical results suggest that canola should be dried using air with 60–70% relative humidity and temperatures up to 40°C. Further research is needed to investigate the effect of drying at high relative humidities on canola quality.

ACKNOWLEDGMENT

The experimental data on drying of canola were collected by the senior author while he was at the University of Saskatchewan.

REFERENCES

ASAE. 1987. Moisture measurement—grain and seeds. S352.1. ASAE Standards—1987. Am. Soc. Agric. Eng., St. Joseph, MI 49085.

BALA, B. K., WOODS, J. L. 1984. Simulation of deep bed malt drying. J. Agric. Engng. Res. *30*, 235–244.

BAKKER-ARKEMA, F. W., LEREW, L. E., DE BOER, S. E. and ROTH, M. G. 1974. Grain drying simulation. Research Report No. 224. Michigan State University.

BOYCE, D. S. 1965. Moisture and temperature changes with position and time during drying. J. Agric. Eng. Res. *10*, 333–341.

BRUCE, D. M. 1984. Simulation of multi-bed, concurrent-, counter-, and mixed-flow grain dryers. J. Agric. Eng. Res. *30*, 361–372.

CENKOWSKI, S. and SOKHANSANJ, S. 1988. Mathematical modelling of radial continuous crossflow agricultural dryers. J. Food Process Eng. *10*, 165–181.

CENKOWSKI, S., SOKHANSANJ, S., SOSULSKI, F. W. 1989. Equilibrium moisture content of lentils. Can. Agric. Eng. *31*, 159–162.

CHAU, K. V. 1980. Some new empirical equations for properties of moist air. Trans. ASAE. *23*, 1266–1270.

GALLAHER, G. L. 1951. A method of determining the latent heat of agricultural crops. Agric. Eng. *32*(1) 34, 38.

GORBIS, Z. R. 1964. Heat Transfer in Porous Beds. Moscow.

INGRAM, G. W. 1976. Deep bed drier simulation with intra-particle moisture diffusion. J. Agric. Eng. Res. *21,* 263–272.

JAYAS, D. S., SOKHANSANJ, S. and WHITE, N. D. G. 1989. Bulk density and porosity of canola. Trans. ASAE *32,* 291–294.

O'CALLAGHAN, J. R., MENZIES, D. J. and BAILEY, P. H. 1971. Digital simulation of agricultural drier performance. J. Agric. Eng. Res. *16,* 223–244.

OTHMER, D. F. 1940. Correlating vapour pressure and latent heat data. J. Ind. and Eng. Chem. *32*(6) 841.

OTTEN, L., BROWN, R. B. and VOGEL, K. F. 1989. Thin layer drying of canola. Paper No. 89–6100, Am. Soc. Agr. Eng., St. Joseph, MI 49085.

PABIS, S. and HENDERSON, S. M. 1962. Grain drying theory III: The air/grain temperature relationship. J. Agric. Eng. Res. *7,* 21–26.

PABIS, S. 1982. Teoria Konwekcyjnego Suszenia Produktow Rolniczych (Theory of the Convective Drying of Agricultural Crops). PWRiL, Warszawa.

PICHLER, H. J. 1957. Sorption Isotherms for grain and rape. J. Agric. Engng Res. *4*(2), 159–165.

SHARMA, S. C. and MUIR, W. E. 1973. Simulation of heat and mass transfer during ventilation of wheat and rapeseed bulks. Can. Agric. Eng. *16,* 41–44.

SINGH, D., SOKHANSANJ, S. and MIDDLETON, B. 1983. Drying characteristics of wheat, barley and canola at low temperatures. Paper No. NCR 83–207, Am. Soc. of Agric. Eng., St. Joseph, MI 49085.

SOKHANSANJ, S., CENKOWSKI, S. and JAYAS, D. S. 1987. Equipment and methods of thin-layer drying—A review. Paper No. 87–6556. Am. Soc. Agric. Eng., St. Joseph, MI 49085.

SOKHANSANJ, S., LAMPMAN, W. P. and MACAULAY, J. D. 1983. Investigation of grain tempering of drying tests. Trans. ASAE *26,* 293–296.

SOKHANSANJ, S., SINGH, D. and WASSERMAN, J. D. 1984. Drying characteristics of wheat barley and canola subjected to repetitive wetting and drying cycles. Trans. ASAE. *27,* 903–906, 914.

SOKHANSANJ, S., ZHIJIE, W., JAYAS, D. and KAMEOKA, T. 1986. Equilibrium relative humidity—moisture content of rapeseed canola from 5°C to 25°C. Trans. ASAE. *29,* 837–839.

SUTHERLAND, J. W., BANKS, P. J. and GRIFFITHS, H. J. 1971. Equilibrium heat and moisture transfer in air flow through grain. J. Agric. Engng Res. *16,* 368–386.

THOMPSON, T. L., PEART, R. M. and FOSTER, G. H. 1968. Mathematical simulation of corn during drying—A new model. Trans. ASAE. *11,* 582–586.

LIST OF SYMBOLS

A	=	area	m^2
a	=	parameter	

b	=	parameter	
c	=	specific heat capacity	kJ/(kg K)
c_{ad}	=	specific heat capacity of dry air	kJ/(kg K)
c_{av}	=	specific heat of water vapor	kJ/(kg K)
d	=	diameter of particle	m
G	=	mass of wet grain in a thin layer	kg
G_d	=	dry mass of grain in a thin layer	kg
h_a	=	enthalpy of the air	kJ
h_v	=	average volumetric heat transfer coefficient	kJ/(m^3 K s)
h	=	average surface heat transfer coefficient	kJ/(m^2 K s)
h^*_{fg}	=	latent heat of vaporization of water from moist grain	kJ/kg
h_{fg}	=	latent heat of vaporization of free water	kJ/kg
H	=	humidity of drying air	kgH_2O/kg da.
k	=	drying constant	1/min
λ	=	coefficient of thermal conductivity	kJ/(m s K)
M	=	moisture content	kgH_2O/kg db.
Nu	=	Nusselt number	dimensionless
Re	=	Reynolds number	dimensionless
RH	=	relative humidity	decimal
t	=	temperature	°C
v	=	velocity	m/s
P_v	=	partial pressure of water vapor	Pa
P_{vs}	=	partial pressure of water vapor at saturation	Pa
ϵ	=	porosity of grain	decimal
P_{AT}	=	atmospheric pressure	Pa
Q_a	=	airflow rate	kg/(m^{2}s)
q_s	=	sensible heat	kJ
q_l	=	latent heat	kJ
ρ	=	density	kg/m^3
θ	=	time	s, min
ν	=	kinematic viscosity	m^{2}s
Δ	=	increment	
Ψ	=	sensible heat ratio	decimal

Subscripts

a	=	air
b	=	bulk
d	=	dry
e	=	equilibrium
g	=	grain
i	=	position index for the thin layer
o	=	initial
s	=	sphere which has a kernel dimension

MICROFILTRATION OF CHICKEN PROCESS WATERS FOR REUSE: PLANT STUDIES AND PROJECTED OPERATING COSTS[1]

M. R. HART,[2] C. C. HUXSOLL, L. S. TSAI, K. C. NG,
A. D. KING, JR., C. C. JONES and W. U. HALBROOK

Western Regional Research Center, Agricultural Research Service, U.S. Department of Agriculture, 800 Buchanan St., Albany, CA 94710

Accepted for Publication November 3, 1989

ABSTRACT

Commercial scale ceramic microfilters were used in plant tests to determine flux rate and operating parameters for waters from a poultry scalder, a poultry chiller, and brine from a delicatessen products chiller, under commercial conditions. Filtration produced clear permeate from all waters. Microorganism counts were essentially reduced to zero in scalder and chiller water permeates, with BOD reduced by about 70% in scalder water permeate and about 60% in chiller water permeate. Flux rates were in the range of 224–204 L/m²h for scalder water at 54°C and 114–81 L/m²h for chiller water at ambient temperature. Test results were used to project nonlabor operating savings and/or costs resulting from the use of microfiltration to recondition and reuse bath overflow. For a processing rate of 140 birds/min and bath size of 37,850 L (10,000 gal), an annual savings of $21,000–$26,000 were estimated for scalder water filtration, while annual costs of $65,000–$84,000 were estimated for chiller water filtration. For a deli brine bath size of 1,170 L (300 gal), annual costs of about $700 were estimated. Retentate heating and electrical usage associated with centrifugal filter pumps were projected as predominant cost factors. Besides costs, other factors such as nonchemical control of microbial growth, water savings, and reduced discharge levels may also be important reasons for considering microfiltration.

[1]Reference to a company and/or product named by the Department is only for purposes of information and does not imply approval or recommendation of the product to the exclusion of others which may also be suitable.

[2]Address correspondence to: Marcus R. Hart, Western Regional Research Center, Agricultural Research Service, U.S. Dept. of Agriculture, 800 Buchanan St., Albany, California 94710

INTRODUCTION

The Poultry Industry can save large amounts of water and energy through reuse of certain processing waters. Prior to plucking, chickens are dipped in a scalding water bath kept at about 54°C (129°F). After plucking and evisceration, the birds are cooled to about 4.4°C (40°F) in a chilling bath. A scalder bath overflow of 0.95 L/bird (0.25 gal/bird) is recommended (Brant *et al.* 1982) and federal regulations (U. S. Gov. 1987) require a chiller bath overflow of 1.9 L/bird (0.5 gal/bird) using potable water for make-up. Experience has shown that these flows control microbial populations at safe levels.

A large, well run plant might have a daily (16 h) overflow of about 129,000 L (34,000 gal) or more, of scalder water and 254,000 L (67,000 gal) or more, of chiller water. Both scalder and chiller water may contain as much as 0.15% total solids. Contaminants in scalder water consist of blood, feathers, and feces and other contaminants that may be carried on the bird while contaminants in chiller water are primarily blood and fat. Although reconditioning these overflows is challenging, their reuse would result in substantial water savings and possibly substantial energy savings.

In contrast, brines, used to cool poultry delicatessen products (frankfurters, etc.) to about 4.4°C, are typically discarded in amounts of only a few hundred liters per week. Although relatively insignificant in terms of water usage and energy loss, brine can represent a serious disposal problem because of its salt content, usually about 15%.

Consequently, both processors and governmental agencies have considerable interest in developing safe means of reusing these process waters. Currently, Food Safety and Inspection Service regulations (U. S. Gov. 1987) allow reconditioned water to replace potable water in make-up to poultry chiller baths, in prescribed ratios, provided minimum percent reductions in microorganisms and minimum percent light transmission in the treated water are met.

Diatomaceous earth filtration was found effective for reconditioning poultry process water for reuse by Rogers (1978) and Lillard (1978a, 1978b, 1980). Unfortunately, the amount of diatomaceous earth needed for the large quantities of poultry water involved would be costly and would generate excessive amounts of used diatomaceous earth for disposal.

Microfiltration is an alternate means of removing particulates in the size range where diatomaceous earth is effective and likely could be used in similar applications. Early microfilter membranes were somewhat limited in the range of operating conditions that they could tolerate. However, ceramic microfilters are now commercially available and their inertness and durability enable them to withstand a wide range of operating temperatures and pressures (Hurley 1987; Zanetti *et al.* 1986). Manufacturers specify that filters can operate continuously at pressures up to 1724 kPa (250 psi) and temperatures up to 750°C (1382°F) and can be washed with hot 2% NaOH or hot 2% HNO_3. Ceramic microfilters are expensive, with installed cost of complete units (filter and supporting equipment and instrumentation) generally running about $600–650 per square foot of membrane, but technology to produce these filters is new and still evolving. Consequently, the price of these filters may be reduced in the future as production technology is improved or economies of scale are realized. Hart *et al.* (1988) have investigated the application of ceramic microfilters for filtration of poultry scalding and chilling waters and frankfurter chilling brine in laboratory and pilot scale tests. They found microfiltration to be an effective means of clarifying and eliminating bacteria from these process waters.

The purpose of this study was to examine commercial scale microfiltration of waters used for scalding and chilling poultry and brine used for chilling poultry delicatessen products. Specific goals were to (1) determine flux rates for commercial scale filters under plant operating conditions, (2) verify microbial reduction in the permeate, and (3) estimate energy and nonlabor operating savings by microfiltration over conventional operation based on test results.

MATERIALS AND METHODS

Equipment and Experiments

A test unit was supplied by Norton Co., Worcester, MA., the manufacturer of Cereflo brand microfilters, and installed at a poultry processing plant. The unit was capable of containing up to four microfilter modules in series and included a centrifugal pump to circulate water to the filters, a heat exchanger and temperature controller, and instrumentation to monitor inlet flow rate, inlet and outlet pressure, and inlet temperature. The pump was fixed speed and large enough to handle a variety of test liquids. Filter inlet and outlet valves throttled pump flow and by judicious adjustment of these valves, both retentate flow and pressure was controlled. Permeate was kept at atmospheric pressure in all tests.

Each filter module consisted of a commercial scale Ceraflow sintered alumina microfilter in a stainless steel housing. The microfilter consisted of a bundle of 280 tubes, each 40 cm long by 2.8 mm inside diameter to give a total membrane area of 0.93 m^2 (10 ft^2). Retentate was circulated inside the tubes with permeate passing outward through the porous tube wall. Pore diameter at the inner surface of the tubes was nominally 0.20 μm, increasing to a much coarser diameter outward from the membrane surface.

Near the end of the testing period for this report, an improved filter design became available for use. A pilot scale filter consisted of a single porous cylinder, 40 cm long by 2.1 cm diameter. Nineteen tubular channels or lumens, analogous to tubes in the original filter, extended the length of the cylinder. Retentate was circulated in the lumens with permeate passing through a nominal 0.20 μm pore size lumen surface and outward through the porous cylinder. Lumens were uniformly spaced in cylinder cross section, providing an increasingly longer exit path for permeate from lumens nearer the center of the cross section. A lumen diameter of 2.8 mm, the same as the inside diameter of the tubes, resulted in a total membrane area of 0.06 m^2 (0.64 ft^2). From a filtration standpoint, the tube and lumen designs differed only in the average distance permeate traveled in the coarse membrane backing material before exiting the filter. These two designs will be referred to as tube filter and lumen filter in this report. Porous cylinders in a commercial scale lumen filter were similar in all dimensions to a pilot scale lumen filter except for cylinder length which was 84 cm. In a commercial scale filter module, 22 porous cylinders were mounted in a stainless steel housing, resulting in 418 lumens and a membrane surface area of 3.1 m^2 (33 ft^2). Although a commercial scale lumen filter was briefly tested, all plant tests in this report used a commercial scale tube filter.

In most tests, process water from the plant poultry scalder, poultry chiller, or brine from the poultry delicatessen products chiller (deli brine) was collected and transported a short distance to the plant area housing the test unit. Experiments were begun using scalder or chiller water within a few minutes of their collection. Brine was collected after plant shutdown and held for approximately 8 h at ambient temperature until tests were begun the next morning. Upon arrival at the filter unit, scalder water was passed through a number 12 mesh screen (1.4 mm openings) to remove feathers and miscellaneous larger particulates. Both chiller water and deli brine visually appeared to be relatively free of large particulates and were not screened. Water for treatment was then placed in a 757 L (200 gal) tank. During filter operation, water was continuously circulated from this tank through the filter units and heat exchanger and returned (as retentate). Permeate was withdrawn from the filter and discarded or recombined with retentate, depending on the experiment.

Although no separate heat source was available, the recirculation pump added considerable heat to the water and this was enough to enable temperature control at or near scalder temperature (54°C). Tap water at about 21°C was the only coolant available. Consequently, neither chiller water or deli brine could be held at their normal plant operating temperature; both were filtered at or near ambient temperature (24–30°C).

There was a limited volume of deli brine available. Consequently, deli brine permeate was recombined with retentate in order to conserve the test water. These tests, where permeate and retentate were recombined, are referred to as continuous.

No such volume restrictions applied to the other waters and they were tested in either continuous operation or batch operation. In batch operation, permeate was discarded, causing an increase in particulate concentration of the retentate.

The amount of concentration was calculated as the ratio of total water divided by retentate volume (V_o/V_r). In some batch tests additional process water was added to the retentate in amounts equal to the permeate removed. This was accomplished by repeatedly drawing down retentate volume by 10–20%, then returning it to its original volume by the addition of fresh process water. These tests are referred to as top-off-batch (TOB) tests.

The effect on flux of increasing pressure (a pressure scan) or increasing recirculation rate (a flow scan) was monitored in continuous tests. A pressure scan was made by holding recirculation rate constant at 303 L/min (80 gpm) and varying filter pressure (average between inlet and outlet pressure) between 276–827 kPa (40–120 psi). A flow scan was made by holding filter pressure constant at 276 kPa (40 psi) and varying flow between 151–454 L/min (40–120 gpm). During each scan, pressure or flow was increased in 137.9 kPa (20 psi) or 75.7 L/min (20 gpm) increments. At each new setting, conditions were held constant for about 5 min then flux, inlet temperature and pressure, flow, and outlet pressure was measured. This was repeated until all points in a scan were tested. In order to relate the flow scans to the filter membrane, volumetric flow was converted to linear velocity across the membrane.

To supplement the plant tests, an additional TOB test was made on poultry scalding water at the Western Regional Research Center (WRRC). A pilot scale lumen filter was used in pilot scale equipment similar to that used in plant tests. A sample of water was collected at the poultry processing plant and transported at ambient temperature to WRRC where it was immediately passed through 40 and 325 mesh sieves to remove feathers. Filtration was begun within about 2 h from collection and continued for an extended test of 18 h duration.

During some tests, periodic samples were taken for microbial, BOD, solids, and chemical analyses.

Filters were cleaned at the end of the day or after an extended test, usually after 4–8 h operation. CIP 150 commercial cleaner (West Coast Chemical Co.) was used for cleanup. Cleaner was added to water (permeate, collected during tests, or tap water) according to manufacturers' directions and the cleaning solution circulated through the filters for about ½ h. Filter inlet and outlet valves were opened full and permeate withdrawal ports sealed during cleaning. Temperature of the cleaning solution usually rose to 54–71°C (130–160°F) during recirculation. The system was then flushed with permeate.

Analyses

BOD, turbidity and plate counts from the plant tests were done by the plant quality control unit of the poultry processor using standard procedures (EPA 1979; APHA 1980). Plate counts from the pilot scale test were done at WRRC by plating samples on nonselective Plate Count Agar and aerobically incubating at 25°C for four days. Total solids, ash, fat, and Kjeldahl nitrogen were determined by AOAC methods (AOAC 1975) at WRRC.

Projected Operating Costs

The change in nonlabor operating costs resulting from microfiltration of bath waters was projected for a hypothetical plant operating within normal industry operating parameters. Costs were based on 16 h/day, 5 days/week, and 52 weeks/year operation. Utility and sewage rates were those available in part of California during the summer of 1987. Fresh water was supplied by a local utility at 15.5°C (60°F). A processing rate of 140 birds/min was assumed, with a plant total water usage of 8 gal/bird. Yearly average electrical rate was \$0.09196/Kw-h, natural gas was \$4.16/MBtu, and the incremental water rate (at plant usage of 23.3 Mgal/month) was \$0.08/100,000 gal. Sewage charges were based on an annual capacity charge of \$16,000/Mgal average daily discharge, and a monthly charge of \$105/Mgal. Both capacity and use charges for biological oxygen demand (BOD) and suspended solids (SS) existed, but were based on pounds discharged rather than discharge concentration. It was assumed that retentate was discharged to plant effluent after microfiltration, keeping pounds of BOD and SS from the plant unchanged. The same amount of BOD and SS would be discharged resulting in higher concentration, but plant effluent volume would be reduced about 10%. Consequently, sewage plant capacity would not be adversely affected. According to a sewage utility spokesperson, BOD and SS charges would be unchanged in this case.

Figure 1 illustrates a hypothetical microfilter installation used for projecting costs for either a scalder bath or a chiller bath. Costs were based on bathwater either being discarded or saved as permeate at the end of the day. At start-up, the bath was filled with stored permeate or fresh water. Fresh water was added to produce overflow until microfiltration was started. Overflow was used to fill a retentate tank. One of two filter sets was started as soon as the retentate tank was filled. Permeate was sent to the permeate tank which was sized to equal bath volume. Permeate was returned to the bath and supplied at a constant rate equal to the bath overflow. Initial filter flux was such that permeate accumulated in the permeate tank. As flux rate dropped with time, permeate volume in the tank dropped towards zero. When near zero, filtration was switched to the clean filter set and the dirty set cleaned. Each cycle in this mode was assumed to be equal duration except for the last cycle of the day. If the bath water was to be discarded, the last filter cycle was run until enough permeate was accumulated to supply makeup until the end bath operation. If the bath water was to be saved, it was drained to the retentate tank upon bath shutdown. Filters were kept running to supply makeup until the end of bath operation plus an additional time to

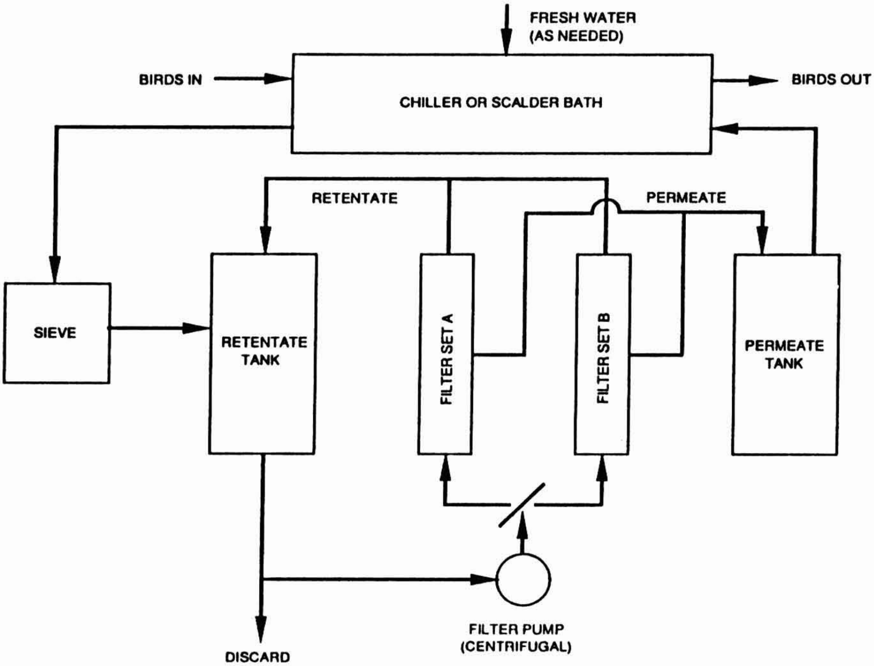

FIG. 1. SCHEMATIC OF PROJECTED MICROFILTRATION SYSTEM FOR USE WITH POULTRY SCALDER OR CHILLER BATH WATER

accumulate permeate equal to bath volume. Permeate was stored in its tank until used to fill the bath at the start of the next working day. In both cases, retentate was discarded when filters were shut down. Cleaning was assumed done in place with filter pumps operating ½ h for each cleaning cycle. Cost of pump operation for cleaning was included but cost of cleaning chemicals was assumed low and ignored.

A bath size of 37,850 L (10,000 gal) was assumed for a scalder bath, with an overflow requirement of 0.25 gal/bird. Overflow temperature was 54°C and overflow was assumed to be sieved, with sieve operating costs low enough to be ignored in these projections. The retentate tank was sized such that concentration ratio at the end of the day would reach 25.

Chiller bath size was also assumed to be 37,850 L (10,000 gal), with an overflow requirement of 0.5 gal/bird. Overflow was either at 15.5°C or at 1°C (34°F). The retentate tank was sized such that concentration ratio at the end of the day would reach 10.

The arrangement in Fig. 1 was modified somewhat for a deli brine chiller. Because no overflow was required and a much smaller volume was involved, microfiltration was assumed to be started after the end of daily brine chiller operation. A bath size of 1135 L (300 gal) was assumed for a deli brine chiller. Upon chiller shutdown, brine was drained to the retentate tank which was equal to the bath size. Filtration was begun, using a single filter set, and continued until retentate volume was 10% of chiller bath volume. Filtration was stopped and retentate discarded. Permeate was stored in its tank and then used to fill the chiller before chiller start-up.

In calculating operating costs, it was assumed that all process waters were filtered at a pressure of 276 kPa (40 psi) and at the same flows used in plant tests, 4.4 m/s for scalder water, 3.6 m/s for chiller water, and 2.9 m/s for deli brine. Flux rates were the same as those obtained in plant or pilot scale TOB or extended runs; flux was completely restored after cleaning, and concentration of particulates in retentate had negligible effect on flux rate at the dilute concentrations involved. Where filtration was projected at temperatures lower than that used in actual testing, it was assumed that flux was proportional to viscosity of water and measured flux rates were multiplied by the ratio of pure water viscosity at the tested and projected temperatures to obtain a projected flux rate. Fuel conversion efficiency was assumed to be 80% for boiler steam and 90% for steam heating, giving a combined fuel conversion efficiency of 72%. Cooling efficiency was assumed to be 1.2 Kw-h/ton of refrigeration. Permeate heat loss or gain due to miscellaneous causes was 5% after addition of filter pump heating.

RESULTS AND DISCUSSION

Plant Studies

The tube filter proved to be somewhat fragile and mechanical failure by breakage of individual filter tubes occurred at an unacceptable rate during the testing period. The lumen filter was much more rugged and no failures occurred during limited commercial scale testing or in extensive laboratory scale testing at WRRC, where it was used primarily in other applications not related to this study. All data presented in this report is from the commercial scale tube filter except for one extended pilot scale test using the pilot scale lumen filter with scalder water. Flux from the two designs appeared similar, but testing was too limited to permit a direct comparison.

Removal of feathers from scalder water was essential for effective operation of the filters. During sieving, some feathers were pointed so that quill diameter enabled them to pass the sieve. Because of crossflow filter operation, its unlikely any feathers reduced flux by adhering to the membrane surface. But some feathers oriented such that they laid flat against the filter inlet rather than passing on through. Even though the rate of feathers passing the sieve was low, continuous recirculation of retentate eventually caused a mat of feathers to form and reduce flux by severely restricting filter flow and pressure. To be safe, water must be screened through a sieve with openings small enough to reject all feathers regardless of their orientation.

Figure 2 shows typical pressure and flow scans obtained for the three different types of water. However, they represent a limited number of tests under plant conditions, and were done primarily to establish reasonable operating conditions for plant tests. Further testing would be needed to establish optimum flow and pressure conditions. All three waters gave a relatively flat response to increasing pressure, with both scalder and chiller water showing a slight flux increase with pressure and deli brine a somewhat greater response up to 552 kPa. Above 552 kPa, little increase in flux occurred for either scalder or chiller water while deli brine flux decreased.

Deli brine and chiller water also showed a relatively flat response to increasing flow. However, scalder water showed a steady increase with increasing flow throughout the range tested.

Pressure drop over the length of two tubular filter modules in series (not shown in Fig. 2), showed only small change with increasing pressure during the pressure scans. Pressure drop was 55–69 kPa for scalder water, 83–110 kPa for deli brine, and about 138 kPa for chiller water. However, during the flow scans, pressure drop was strongly affected by increasing flow rate. Pressure drop was 41–124 kPa for scalder water, 55–124 kPa for chiller water, and 55–165 kPa for deli brine.

Figure 3 shows typical extended TOB runs using scalder and chiller water. For scalder water filtered at 50°C, 552 kPa, and 4.39 m/s, flux generally varied between 224–204 L/m^{2}h over the test with the concentration ratio increasing to 6.2. For chiller water filtered at ambient temperature, 552 kPa, and 3.66 m/s, flux varied between 114–81 L/m^{2}h with the concentration ratio increasing to 3.3. Under these conditions, per pass recovery varied between 1.53–1.39% for scalder water and between 0.93–0.66% for chiller water.

Previously reported pilot scale TOB tests on poultry scalder and chiller water (Hart *et al.* 1988) were run at substantially lower pressures, about 110–124 kPa vs 552 kPa for plant tests, but at relatively similar flow rates. Reported flux values of 220–179 L/m^{2}h for scalder water and 110–73 L/m^{2}h for chiller water, were reasonably similar to those obtained in plant tests.

Figure 4 shows the change in flux with time in an 18 h pilot scale test. The test showed that scalder water could be filtered continuously in TOB mode over a two shift timespan (18 h) and that a high concentration ratio could be achieved with an effective flux.

A lumen filter was used in this test. Using a flow rate of 6.04 m/s, which was higher than that used in plant tests, flux remained above 204 L/m^{2}h for about

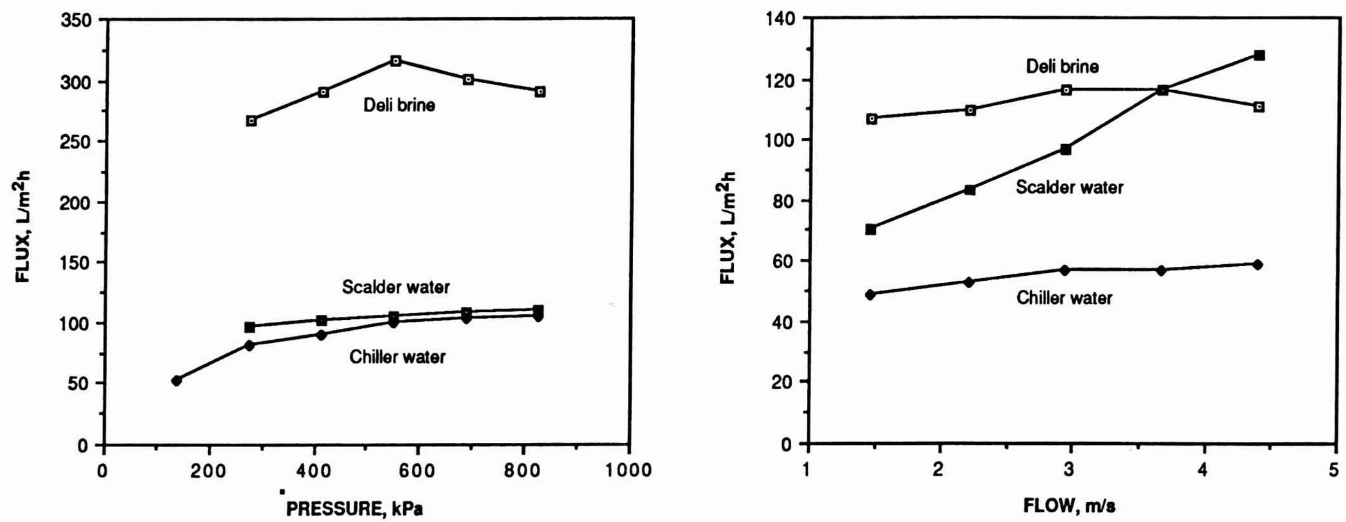

FIG. 2. EFFECT OF PRESSURE AND FLOW CHANGE ON CHICKEN PROCESS WATER FLUX USING TUBE FILTER
Left figure shows effect of change in pressure, holding flow constant at 2.9 m/s. Right figure shows effect of change in flow, holding pressure constant at 276 kPa. Filtration of chiller water and deli brine done at ambient temperature and scalder water at 50°C.

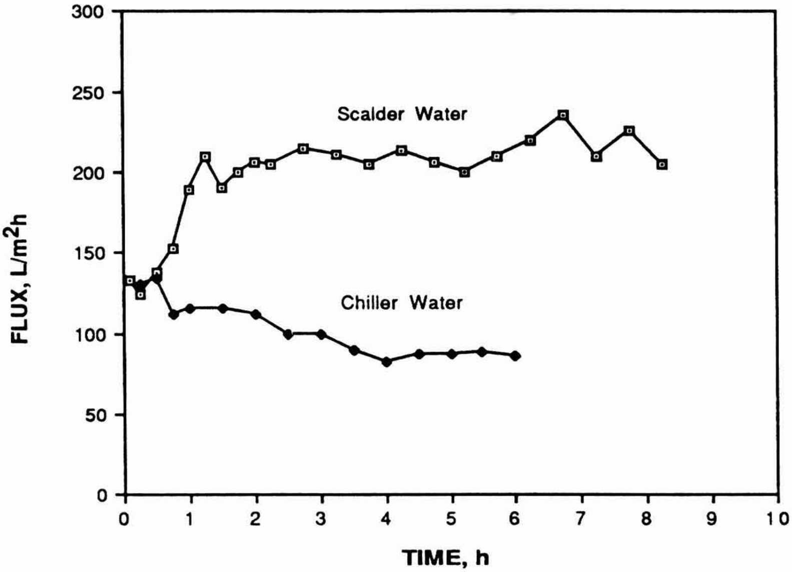

FIG. 3. CHANGE IN FLUX WITH TIME FOR CHICKEN SCALDER AND CHILLER WATER TOP-OFF-BATCH TESTS
Scalder water filtered at 50°C, 552 kPa, and 4.39 m/s, and chiller water filtered at ambient temperature, 552 kPa, and 3.66 m/s using tube filter.

12 h, while concentration ratio increased to slightly more than 18 during this period. After 18 h, flux was still about 183 L/m^{2}h while concentration ratio had increased to 25.2. Recovery per pass varied between 0.59–0.43%, lower than recoveries obtained in plant tests done at lower flow rates. These flux rates are as good or better than most of the plant results. To some extent, the higher flow rate used for this test may have offset any flux reduction caused by the lumen filter design and the increasing particulate concentration.

Initial flux rates for deli brine filtering at ambient temperature were high, but flux rapidly fell to about 81 L/m^{2}h within the first hour of operation. At normal brine chiller temperatures, flux would be expected to be lower. Although brine contained a haze prior to filtration, it visually appeared to be cleaner before filtering than either of the other waters tested. However, it's flux dropped more rapidly and to a lower level than that obtained for either of the other waters, indicating the presence of enough particulates to substantially affect filter performance.

Microfiltration produced clear permeate from all waters. Table 1 shows the effect of filtering on scalder and chiller water characteristics. For both waters,

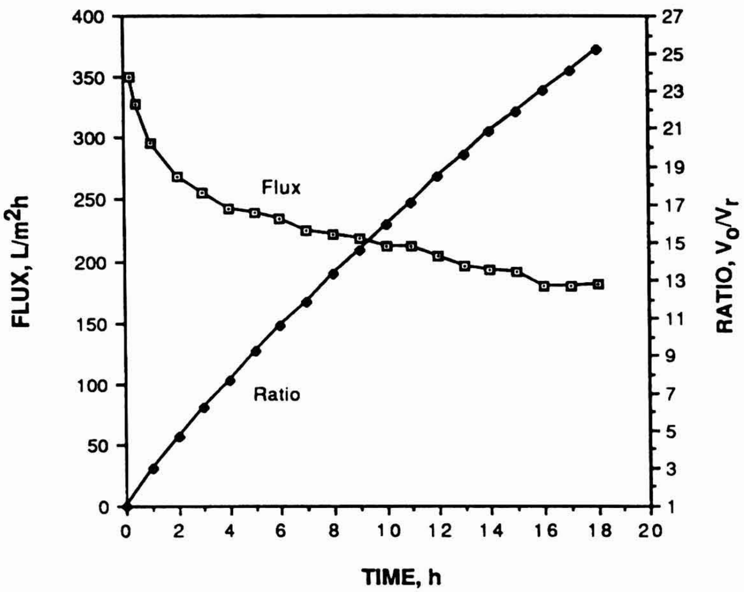

FIG. 4. CHANGE IN FLUX AND CONCENTRATION (RATIO OF TOTAL WATER TO RETENTATE) WITH TIME FOR CHICKEN SCALDER WATER DURING 18 H PILOT SCALE TOP-OFF-BATCH TEST
Filtration at 50°C, 76 kPa and 6 m/s using lumen filter.

starting BOD was about 600 mg/L or more, and starting turbidity about 80 NTU or more. Filtering reduced BOD by 60% or more, and turbidity by 85% or more. Microorganism counts in the permeate, as shown in Table 2, were about 20 or less for plant tests. In the 18 h laboratory pilot scale test, the final count was 10. The 12 h count was about 1600, but since the 18 h count was down to 10, this probably reflects contamination in handling the sample rather than a leak in the filter. Permeate always gave negative indication of Salmonellae presence.

Table 3 lists the composition of scalder water, and permeate and retentate values at various times during the 18 h laboratory pilot scale test. As the concentration ratio of the retentate increased to 25.2, concentration of particulates unable to pass the filter must have increased by this amount. The increase of particulates in the retentate caused the total solids content to increase to almost 1% by the end of the test. Ash, nitrogen and fat content of the retentate increased with time with fat increasing almost 30 fold to about 0.06%. On a dry basis, retentate solids consisted of about 73% crude protein, 6% fat and 14% ash after 18 h filtration.

Fat content of the permeate dropped to zero after 6 h. Nitrogen and ash content of the permeate remained constant throughout the test.

TABLE 1.
CHARACTERISTICS OF SCALDER AND CHILLER WATER

Sample	BOD mg/L	Turbidity, Nephelometric turbidity units.
Scalder Water		
Plant run 3/23/87		
Starting water	598	81
Permeate	189	11
Chiller Water		
Plant run 3/24/87		
Starting water	650	87
Permeate	258	8

Projected Operating Costs

Most of the space required for microfiltration would be for tanks containing retentate and permeate. The bundled tube or lumen configuration of microfilter modules is a compact design, using minimal floor space for filter units. The test unit in this study (excluding tanks) could house up to 6.1 m^2 (66 $ft.^2$) of membrane and occupied about 2 m^2 of floor space. Larger units would probably be more space efficient.

Based on the plant and pilot scale data obtained and the assumptions outlined in the Materials and Methods section it was assumed that a total membrane area of 61.3 m^2 was needed for a scalder installation, 297.3 m^2 for a chiller operation at 15.5°C, 445.9 m^2 for a chiller operation at 1°C, and 3.72 m^2 for a deli brine operation. This assumes only half the membrane area is in use for scalder or chiller operations at a given time. Based on a cost of \$600/ft^2 of membrane, capital cost would be \$396,000 for a scalder installation, \$1,920,000 for a chiller operation at 15.5°C, \$2,880,000 for a chiller operation at 1°C, and \$24,000 for a deli brine operation. Substantial operating savings would be needed to justify these capital costs, especially in the case of chiller water microfiltration.

Microfiltration would probably be automated, thus labor costs would be based on monitoring and servicing the equipment and would probably be minimal. These considerations, plus others involved in determining total cost of a microfiltration system were beyond the scope of this study. However, changes in energy usage and nonlabor operating costs, resulting from microfiltration, were estimated to determine possible savings in these areas over conventional operation.

TABLE 2.
MICROORGANISM CONTENT OF PROCESS WATERS

Sample	[a]V_o / V_r	Total Micro-orgainsms/ml	Coliform Micro-organisms/ml	Salmonellae
Scalder Water				
Plant run 3/23/87				
Starting water	1.0	6.1×10^5	- -	negative
Permeate[b]	1.0	21	- -	negative
Plant run 3/31/87				
Starting water	1.0	3.6×10^7	- -	positive
Permeate[b]	1.0	2	- -	negative
Plant run 9/15/87				
Retentate	5.7	1.1×10^7	$<10^5$	negative[d]
Retentate	5.7	2.4×10^7	$<10^5$	negative[d]
Permeate[c]	5.7	0	0	negative
Permeate[c]	5.7	1	0	negative
Lab run 10/14/87				
Starting water	1.0	2.63×10^4	- -	- -
6 Hours running				
Retentate	10.6	5.37×10^4	- -	- -
Permeate[c]	10.6	182	- -	- -
12 Hours running				
Retentate	18.4	1.82×10^6	- -	- -
Permeate[c]	18.4	1622	- -	- -
18 Hours running				
Retentate	25.2	1.45×10^7	- -	- -
Permeate[c]	25.2	10	- -	- -
Chiller Water				
Plant run 3/24/87				
Starting water	1.0	6.1×10^5	- -	negative
Permeate[b]	1.0	21	- -	negative

a. Ratio total volume to retentate volume.
b. Tube filter.
c. Lumen filter.
d. Damaged organisms present.

Table 4 summarizes the estimated costs and/or savings resulting from the use of microfiltration in a hypothetical operation. They are based on experimental flux values at particular pressures and flows. Projections would be similar for any equipment with similar characteristics, regardless of supplier.

Filtration of scalder water produced an annual energy savings estimated to be as large as 6604 GJ (gigajoules) when scalder bath water was saved. Heating

TABLE 3.
COMPOSITION OF SCALDER WATER, PERMEATE AND RETENTATE AT VARIOUS TIMES DURING LABORATORY 18 H CONTINUOUS RUN

Sample	[a] V_o/V	% Total Solids	% Ash	% Nitrogen	% Fat
Starting water	- -	0.172	0.053	0.033	0.002
6 Hours running					
Retentate	10.6	0.496	0.087	0.067	0.021
Permeate	10.6	0.105	0.045	0.028	0.006
12 Hours running					
Retentate	18.4	0.808	0.116	0.103	0.048
Permeate	18.4	0.096	0.056	0.027	0
18 Hours running					
Retentate	25.2	0.999	0.136	0.116	0.059
Permeate	25.2	0.084	0.054	0.028	0

a. Ratio total volume to retentate volume.

by centrifugal filter pumps was determined to be one of two major factors affecting operating economics. For scalder water this heating was beneficial, adding an estimated 3–4% of energy in the saved permeate. Losses to ambient surroundings were estimated at 5% after pump heating. Thus, pump heating approximately offset losses to ambient surroundings. Net annual energy savings were estimated at \$27,257 to \$35,415 (1987 dollars). All energy savings were corrected to reflect the estimated efficiency for energy replacement. Thus the net energy savings are based on the total amount of fuel used to replace the energy lost when overflow and bath water are discarded.

Scalder water usage was estimated to be reduced by 31700–37800 m^3/year with a corresponding reduction in sewage discharge. This resulted in combined savings for sewage and water of up to \$2683/year. Only about ⅓ of these savings are attributable to water savings.

Filter pump electrical usage was the largest cost factor. Electrical usage for pumping was estimated as large as \$11,801/year. Overall, net operating savings for microfiltration of scalder water was estimated to be from \$20,607 to \$26,297 annually.

For the poultry chiller, an overflow temperature of 15.5°C was the same as make-up water temperature. Consequently, there was no energy (refrigeration) saved by saving overflow water. When bath water was also saved, its average temperature was lower than makeup water and an estimated 90 GJ/year of refrigeration was saved. For a chiller operated at 1°C overflow, estimated energy savings as large as 4139 GJ/year of refrigeration might be achieved.

TABLE 4.
SUMMARY OF ADDITIONAL ANNUAL OPERATING COSTS OR SAVINGS RESULTING FROM MICROFILTRATION

Operation	GJ Saved by filtration	GJ added by Pumping	Net[a] Energy Savings or (Costs)	Saved Water m^3	Water & Sewage Savings	Pumping Cost	Overall Net Savings or (Costs)
POULTRY SCALDER							
Bath discarded end of day	5089	150	$27,257	31737	$2,067	$8,717	$20,607
Bath saved end of day	6604	203	$35,415	37854	$2,683	$11,801	$26,297
POULTRY CHILLER							
15.5° C Bath Overflow							
Bath discarded end of day	0	928	($7,688)	59538	$3,878	$61,419	($65,228)
Bath saved end of day	90	1092	($8,295)	68395	$4,455	$70,917	($74,757)
1° C Bath Overflow							
Bath discarded end of day	3597	1403	$18,179	59538	$3,878	$92,752	($70,695)
Bath saved end of day	4139	1679	$20,380	68395	$4,455	$108,760	($83,925)
DELI BRINE CHILLER	2.9	10.2	($63)	533	$2	$628	$(689)

a. Adjusted for estimated 5% heat loss or gain.

However, because of lower flux rates, chiller retentate was recirculated much more than scalder retentate and more heat was added by pumping. Centrifugal filter pump heating subtracts from the refrigeration saved and, for 15.5°C overflow, resulted in more heat being added than refrigeration was saved for a net energy cost of as much as $8,295. In contrast, 1°C overflow, with larger energy savings, saved as much as $20,380 in net energy savings.

Pumping costs were the largest costs in chiller microfiltration economics with costs varying from $61,419 to $108,760. This far outweighed all other costs or savings and resulted in an estimated overall net cost of $65,229 to $83,925 annually.

Deli brine chiller operations involved very small savings or costs relative to the large volume operations of poultry scalder or chiller microfiltration. As in the poultry chiller operation, heat added by the centrifugal filter pump was substantially greater than refrigeration saved but the corresponding estimated net energy cost was only $63 annually. Water and sewage savings were negligible. Pumping cost was estimated at $628/year for an overall cost of $689.

Thus overall microfiltration operating economics result in a savings for scalder water and increased costs for chiller water and deli brine. Because of the large capital costs involved, microfiltration is unlikely to be used unless capital costs are reduced, improvements in operating savings can be made, especially for microfiltration of chiller water, or other noncost or regulatory factors assume greater importance.

In looking for process improvements, pumping is the overwhelming negative process factor. It directly adds large costs through electrical charges and indirectly adds costs through heating of chiller waters and brines. Pumping requirements are determined by flux rate. Increasing chiller water and brine flux rates would decrease the recirculation needed, reducing both electrical costs and permeate heating. One approach to increasing flux rates might be to preclean process water before microfiltration, using flocculation or other techniques to reduce the amount of particulates.

An approach to reduce pump heating is to substitute positive displacement pumps for centrifugal pumps. This would reduce or eliminate the heating due to liquid slippage around centrifugal impellers. However, positive displacement pumps are usually more expensive to buy and maintain.

Another consideration is the cost of fuel. As fuel costs rise, the economics of scalder water microfiltration would probably be improved since there is a net energy savings involved although pumping costs (electrical) would also be increased. Chiller waters or brines, however, would be much more expensive to filter, since there is a large negative energy saving involved in addition to increased pumping costs.

Increased water or sewage costs are unlikely to affect overall economics of the process since they would still likely be a small portion of the savings.

However, if plant water usage approached supply limits, or if discharge approached regulatory limits, microfiltration could become important in holding plant operation below critical limits.

Perhaps the most important noncost factor for consideration is the role that microfiltration could play in controlling bacterial growth. It has been shown that above certain dosage levels (Masri 1986; Tsai *et al.* 1988), chlorination causes the formation of undesirable compounds in chiller waters. While this has not been shown to make poultry less safe, it is possible that future safety considerations may limit the use of chlorine or other similar bactericides.

Microfiltration can be used as the primary agent for control of bacterial growth by filtering process water at a rate sufficient to keep bacteria at acceptably low levels. Alternately, if chlorine or other bactericides or inhibitors are used, microfiltration may reduce dosage needed since filtration would remove microorganisms, and disinfectant, normally discarded in the overflow, would be returned to the bath in reused permeate. An added benefit of reduced or eliminated chlorination would be the saving of chlorine costs and decreased chlorine induced equipment corrosion. No dollar value was assumed for this in the operating projections of this report but would certainly be a positive factor in a more detailed analysis.

SUMMARY AND CONCLUSIONS

Commercial scale ceramic microfilters were used in plant tests to determine flux rate and operating parameters under commercial conditions. Screening to remove occasional feathers from scalder water was found to be essential for efficient filtration. Filtration produced clear permeate with microorganism counts essentially reduced to zero and BOD reduced by about 70% in scalder water permeate and about 60% in chiller water permeate. For all waters tested, flux showed only small increases as filter pressure was increased while holding flow constant. When flow was increased while holding pressure constant, scalder water flux strongly increased, but both chiller water and deli brine flux showed very little increase. For all waters, pressure drop was essentially unchanged by increasing filter pressure but was strongly affected by increasing flow. In TOB tests, flux rates were in the range of 224–204 L/m^2h for scalder water and 114–81 L/m^2h for chiller water. These results are similar to those determined in laboratory tests for scalder and chiller waters. Rates for deli brine were around 81 L/m^2h. In an 18 h, pilot scale TOB test, using scalder water, a concentration ratio of 25.2 was achieved.

Test results were used to project energy and nonlabor operating savings resulting from using microfiltration in conjunction with a commercial scale poultry scalder, poultry chiller, and brine chiller for delicatessen products. Projections were based on a processing rate of 140 birds/min and a microfiltration pressure of 276 kPa. Use of microfiltration was projected to result in operating savings of about \$21,000–\$26,000 annually for scalder water, but result in increased operating costs of about \$65,000–\$84,000 annually for chiller water and about \$700 annually for deli brine. Because of the large capital costs involved, microfiltration is unlikely to be used unless improvements in capital costs or operating savings can be made, or noncost or regulatory factors become more important.

Retentate heating and electrical usage associated with filter pumps were the predominant operating cost factors. In general, microfiltration of cooled waters will be less attractive than microfiltration of heated waters because of heat added to the waters by pumping and depression of flux rates associated with lower temperature filtration. Improving flux rates reduces pumping and thus reduces both pump heating and electrical usage.

Additional factors besides capital and operating costs or savings may become important in considering microfiltration. Such factors as water availability, waste discharge limits, and changes in the regulation of chemical disinfectants may encourage future use of microfiltration to alleviate these problems.

REFERENCES

AOAC. 1975. Official Methods of Analysis (12th ed.), Assoc. Official Agricultural Chemists, Washington, D.C.

APHA. 1985. Standard Methods for the Examination of Water and Wastewater, 16th Ed. APHA, AWWA and WPCF, Washington, D.C.

BRANT, A. W., GOBLE, J. W., HAMANN, J. A., WABECK, C. J. and WALTERS, R. E. 1982. Guidelines for Establishing and Operating Broiler Processing Plants. U.S. Dept. Agric. Agricultural Research Service. Agriculture Handbook No. 581.

EPA. 1979. Methods for Chemical Analysis of Water and Wastes. U.S. Environmental Protection Agency, publication EPA-600/4-79-020.

U.S. GOV. 1987. Code of Federal Regulations, Title 9, Section 381.66.

HART, M. R., HUXSOLL, C. C., TSAI, L. S. and NG, K. C. 1988. Preliminary studies of microfiltration for food processing water reuse. J. Food Prot. *51,* 269–276.

HURLEY, P. 1987. New filters clean up in new markets. High Technol. Aug. pp. 21–24.

LILLARD, H. S. 1978a. Improving quality of bird chiller water for recycling by diatomaceous earth filtration and chlorination. J. Food Sci. *43,* 1528–1531.

LILLARD, H. S. 1978b. Evaluation of broiler necks flumed with diatomaceous earth filtered chiller water. J. Food Sci. *43,* 1532–1534.

MASRI, M. S. 1986. Chlorinating poultry chiller water: The generation of mutagens in water reuse. Fd. Chem. Toxic. *24,* 923–930.

ROGERS, C. J. 1978. Recycling of Water in Poultry Processing Plants. U.S. Environmental Protection Agency, Report EPA-600/2-78-039.

TSAI, L. S., MAPES, C. J. and HUXSOLL, C. C. 1988. Aldehydes in poultry chiller water. Poultry Sci. *66,* 983–989.

USDA. 1973. Meat and Poultry Programs, meat and poultry inspection regulations. Animal and Plant Inspection Service, U.S. Dept. Agriculture.

ZANETTI, R., SHORT, H., HUNTER, D. and USHIO, S. 1986. Ceramics make a strong bid for tough membrane uses. Chem. Engr. *93,* 19–22.

HEAT TRANSFER DURING EVAPORATION OF MILK TO HIGH SOLIDS IN THIN FILM SCRAPED SURFACE HEAT EXCHANGER

A. K. DODEJA, S. C. SARMA and H. ABICHANDANI

National Dairy Research Institute
Karnal-132001 (India)

Accepted for Publication November 29, 1989

ABSTRACT

Thermal performance of thin film scraped surface heat exchanger was evaluated for concentration of milk to high solids with process variables such as mass flow rate, steam condensing, temperature, etc. Appropriate dimensionless groups were formulated and fitted in Cobb-Douglas model to obtain a correlation. This relationship which is in the form of a Nusselt equation will be useful in predicting the scraped film coefficient during milk concentration to high solids. The effect of process variables on scraped film coefficient were discussed.

INTRODUCTION

Several heat transfer problems are encountered in processing of milk and its products. Because of wide range of rheological properties associated with milk and its products, severe fouling results when they are processed in conventional heat exchangers. This imposes restrictions on the operating temperatures and time. This problem can be overcome by employing the simple method of scraping the heat transfer surface continuously. In this technique the slow moving layer at the surface which restricts the rate of heat transfer is rapidly removed and mixed with bulk of liquid. Simultaneously fresh product is brought into contact with heat transfer surface. The action of blades substantially accelerates heat and mass transfer rates by creating turbulence and pumping action. This mechanical agitation safeguards against fouling, greatly reduces the width of residence time distribution (RTD).

The scraped surface heat exchangers (SSHE) can be distinguished by two modes of operation.

(1) Liquid full operation—when the heat exchanger contains a pool of liquid.
(2) Thin film operation—In this case the liquid moves along the heat transfer surface as a thin film.

The thin film scraped surface heat exchanger can further be classified as:

(a) Wiped film unit—Where a fixed gap exists between the rotating blades and the heat transfer surface.
(b) Scraped thin film unit—Where the clearance between the blades and heating surface varies.

It has been claimed that a thin film SSHE with rotor having swinging blades has a wider field of application as compared to one with fixed blades (Skoczylas 1970). It was reported that swinging blade type of SSHE can even deliver final product in form of a solid (Hauschild 1969). The heat transfer depends not only on the liquid flow rates but also on the rotor speed, mass of blade and diameter of heat exchangers. Freeze and Glover (1979) have summarized several unique performance characteristics of mechanically agitated thin film evaporator.

The technology of application of SSHE attained its well deserved position in distillation, concentration, drying, etc., and even in accelerating chemical reactions. In the chemical, pharmaceutical, food, polymer and other industries, thin film units are used successfully for processing of products which otherwise cannot be handled economically or reliably.

Angell and Baird (1983) conducted a study on processing of radioactive wastes with SSHE to produce concentrated slurries with 50% or more solids. The study covered continuous volume reduction of miscellaneous suspended solids, oils, calcium salts and detergent in water.

Abichandani and Sarma (1987) evaluated performance of thin film SSHE using milk and cream as working fluids. The study observed that overall heat transfer coefficient increased with increasing rotor speed and in particular its change was rapid when speed was increased from 2.67 m/s to 3.55 m/s. Increasing the rotor speed beyond 3.55 m/s was reported to have insignificant effect on overall heat transfer coefficient for fluid with fouling tendencies. This confirms the finding of Bressler (1959).

The dairy industry has so far not considered seriously the potential of thin film SSHE in processing of milk leading to high solids. This paper presents investigations on thin film SSHE for manufacture of milk products, particularly those with high concentration of solids. Such product has several uses in manufacture of milk based sweets etc.

MATERIALS AND METHODS

Theoretical Consideration

When milk is pumped through SSHE at near its saturation temperature entire heat transferred from steam is assumed to cause evaporation of water from milk. The SSHE was insulated with glass wool. The thickness of insulation was so chosen that outside surface temperature of SSHE was same as ambient temperature. Thus

$$Q = U_o A_o \Delta T \tag{1}$$

Where $\Delta T = T_s - T_l$

$$\text{and } Q = M_v L_v \tag{2}$$

The thermal performance of thin film scraped surface heat exchanger can be evaluated in terms of overall heat transfer coefficient. The overall heat transfer coefficient constitutes scraped film coefficient, metal wall resistance and steam film coefficient. It can be expressed in form:

$$\frac{1}{U_o} = \frac{1}{h_o} + \frac{D_o}{D_l}\frac{1}{h_s} + \frac{D_o}{2\,K_m}\ln\frac{D_o}{D_i} \tag{3}$$

For a scraped surface heat exchanger of fixed wall thickness the thermal resistance of the wall will have fixed value. The steam film coefficient for condensing steam on horizontal pipe is given by Nusselt's relationship (McAdams 1963).

$$h_o = 1.51\,\text{Ø}\left[\frac{4\,T}{\mu_f}\right]^{-1/3} \tag{4}$$

Where T is mass flow rate of condensate from the lowest point divided by heated length.

$$\text{and Ø} = \left[\frac{k^3\rho^2 g}{\mu_f^2}\right]^{1/3} \tag{5}$$

Where k = thermal conductivity of condensate
ρ = density of condensate
μ_f = absolute viscosity of condensate
g = gravitational acceleration.

All the above properties are corresponding to film temperature.

Flow behavior of milk changes from Newtonian to pseudoplastic during concentration to high solids (Sawhney and Kumar 1984). Therefore the flow can be defined by:

$$\pounds = m\,(-du/dy)^n \tag{6}$$

Where m = Flow behavior Index
n = Consistency coefficient
£ = Shear stress

Based on this consideration the scraped surface film coefficient can be considered as a function of following parameters and expressed in the form:

$$h_s = f\,(M_p, T_s, B, N, S, m, n, C_p, k) \tag{7}$$

Abichandani (1985) in his work on evaporation of buffalo milk showed that optimum overall heat transfer coefficient was achieved by keeping a circumferential velocity in range of 2.67 to 3.55 m/s and number of blades as four. When number of blades and rotor speed are selected, according to this observation the scraped film coefficient can be expressed in a similar form:

$$h_s = f(M_p, T_s, S, m, n, C_p, k) \tag{8}$$

Since total solids at the outlet of SSHE depends on mass flow rate of product, the relationship can be further reduced to the form:

$$h_s = f(M_p, T_s, m, n, C_p, k) \tag{9}$$

In terms of dimensionless groups, h_s can be expressed in form:

$$Nu = K\,(NRe)^a_{Ge}\,(Pr)^b_{Ge}\,(\Delta T/T_s)^c \tag{10}$$

The dimensionless groups were computed with average values of physical properties of milk at inlet and outlet conditions (Charm 1959; Harper 1960).

Physical Properties of Concentrated Milk

Specific heat. It was determined from following correlation (Kessler 1981).

$$C_p = x_w \cdot C_w + x_c \cdot C_c + x_p \cdot C_p + x_f \cdot C_f + x_a \cdot C_a \tag{11}$$

Where C stands for specific heat and x for mass fraction of constituent in milk. Subscripts:

p = product
w = water
c = carbohydrates
p = proteins
f = fat
a = ash

Density. It was determined from correlation given below (Agrawala 1973).

$$= 0.9861(S)^{0.045} + 0.002 \text{ Cosech } 1.32\,(55-T) - 0.55 \times 10^{-3}T \quad (12)$$

Where T is bulk temperature, °C, S = total solids, %

Thermal Conductivity. It was determined from following relationship (Fernandez-Martin and Mohtes 1972).

$$k = (b_0 + b_1S) + (b_2 + b_3S)T + (b_4 + b_5S)T^2 \quad (13)$$

Where k = Thermal conductivity in cal.cm/cm^{2}S°C $\times$ 10^4

$$b_0 = 13.21,\ b_1 = -0.0768,\ b_2 = 0.077,$$
$$b_3 = -0.00135,\ b_4 = -0.000507,\ b_5 = 0.0000121$$

Flow Behavior Index and Consistency Efficient. Values at different total solids were taken from literature (Sawhney and Kumar 1984).

Experimental

The schematic diagram of experimental set up is shown in Fig. 1. The feed tank (1) was filled with buffalo milk collected from experimental Diary, NDRI Karnal (Av. composition: Fat 6.6%, Protein 3.9%, Lactose 5.2%, Ash 0.8%, Moisture 84.2%). The steam was admitted to the jacket of feed tank and was maintained at atmospheric pressure. Simultaneously, the agitator was started to ensure uniform mixing and heating. When the milk reached a temperature of 95–96°C, the feed pump (2) was switched on to permit flow of milk into SSHE (4) (ID, 34×10^{-2}m, thickness 0.7×10^{-2}m and 55×10^{-2}m effective length, Material of construction—304 S.S). The temperature of steam in the jacket of SSHE was adjusted to desired value. The flow rate of milk was maintained at desired level by operating valves (V_2) and (V_3). Sufficient flow of tap water was main-

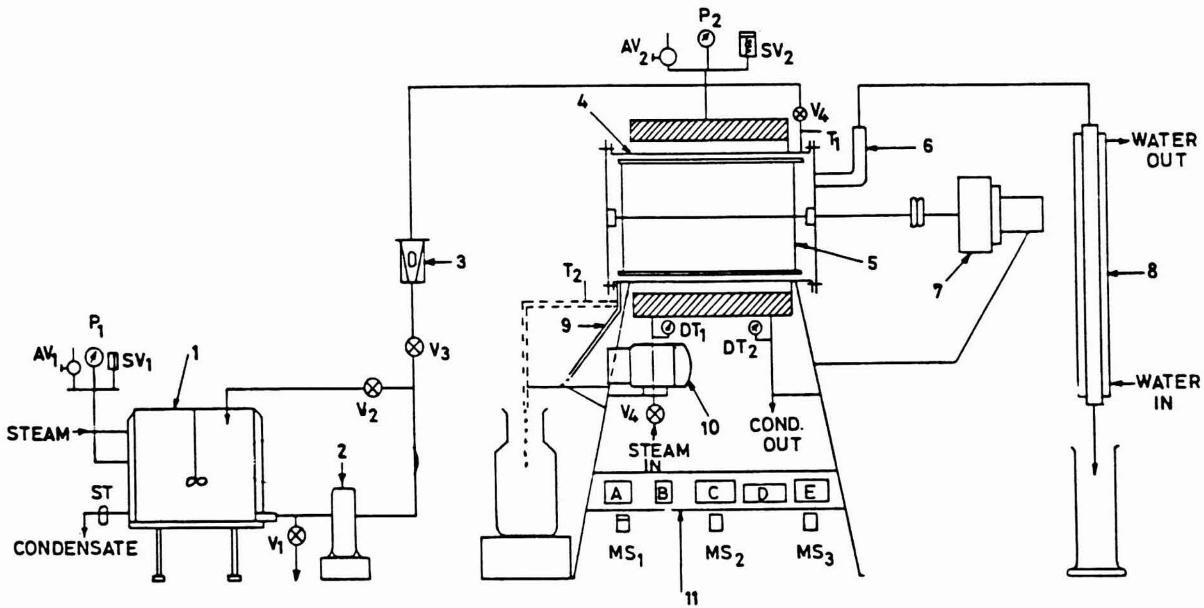

FIG. 1. SCHEMATIC DIAGRAM OF EXPERIMENTAL SET-UP FOR MILK EVAPORATION AND RTD STUDIES

1. Feed tank. 2. Feed pump. 3. Rotameter. 4. Heat exchanger. 5. Scraper. 6. Vapor outlet. 7. Variable speed drive. 8. Condenser. 9. Screw conveyor. 10. Variable speed geared motor. 11. Instrument panel. V_1, V_2, V_3, V_4—Flow regulating valve. ST—Steam trap. T_1, T_2—Inlet and outlet thermo-wells. MS_1, MS_2, MS_3—Motor starters. AV_1, AV_2—Air vents. P_1, P_2—Pressure gauges. DT_1, DT_2—Dial thermometers. SV_1, SV_2—Safety valves. A—Electronic regulator. B—Manual speed controller. C—Selector switch. D—Millivolt meter. E—Watt meter.

tained to condense vapors. The condensate was collected to determine the rate of evaporation. When the steady state was attained, all the process variables were recorded.

Milk was concentrated to various percentage of total solids in the final product by varying mass flow of milk and condensing temperature of steam. Milk was allowed to evaporate at atmospheric pressure. The percentage of solids obtained in the final product varied from 18% to 70%. Condensing temperature of steam was changed from 110°C to 130°C. The mass flow rate of milk was in the range of 9.07×10^{-3} kg/s to 2.53×10^{-2} kg/s. The samples of concentrated milk and raw buffalo milk collected are analyzed for total solids in accordance with the procedure described in ISI 1479 (Part-I).

RESULTS AND DISCUSSION

Experimental data generated during forty trials were grouped into appropriate dimensionless numbers and processed in computer HCL-4 to fit Cobb-Douglas model (Heady and Dillon 1961). Method of least squares was employed in regression analysis to determine intercept constant K and exponents a, b and c of Eq. (10). The following correlation was obtained.

$$Nu = 6615.0619\,(NR_e)_{Ge}^{0.1331}\,(Pr)_{Ge}^{0.0764}(\Delta T/T_s)^{0.2843} \qquad (14)$$

$$19\% \leqslant S \leqslant 70\%$$

No. of blades = 4

$V_c = 3.558$ m/s

Correlation coefficient (R^2) = 0.8492

Standard error of intercept constant = 0.0871

Standard errors of exponents a, b and c are 0.046, 0.051 and 0.051, respectively.

Figure 2 presents the deviation of predicted Nusselt number, $(Nu)_{Pred}$ obtained from above equation from those determined experimentally $(Nu)_{exp}$. The equation seems to be reasonably accurate considering that fairly large number of data are within the range of standard error.

The detailed study of the various process variables on scraped film coefficient predicted by the above correlation will help in understanding heat transfer process in thin film SSHE, during concentration of milk to high solids.

Effect of Steam Condensing Temperature on U_o

Figure 3 illustrates the effect of steam condensing temperature on overall heat transfer coefficient (U_o). The general trend is that overall heat transfer coefficient drops with increasing steam condensing temperature.

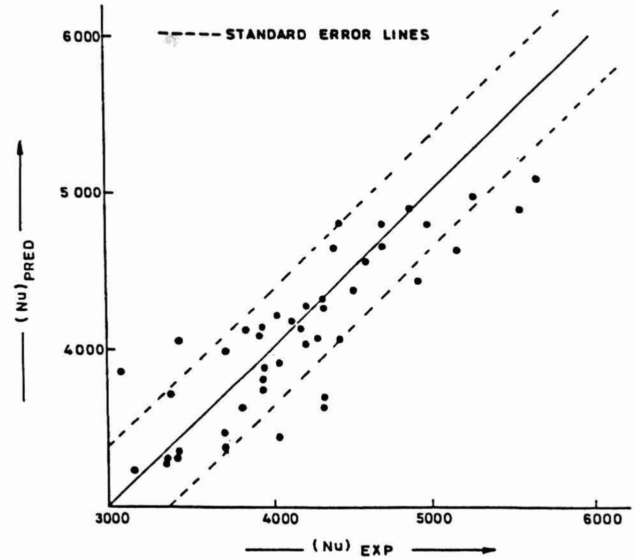

FIG. 2. COMPARISON BETWEEN $(NU)_{EXP}$ AND $(NU)_{PRED}$

The overall heat transfer coefficient given by the Eq. (3) depends upon the steam and scraped film coefficients as the metal wall resistance remains unchanged. Examination of steam film coefficient given by the relationship (4) reveals that as heat transfer rates are increased, the thickness of condensate film increases progressively, causing the steam film coefficient to decrease. It is necessary to examine the effect of condensing temperature on h_s to draw further conclusions. This discussion follows.

Effect of Steam Condensing Temperature on h_s

Figures 4 and 5 illustrate the variation of scraped film coefficient with condensing temperature at various mass flow rates. It can be noticed that when the mass flow rate of milk was between 1.93×10^{-2} kg/s to 2.53×10^{-2} kg/s, the scraped film coefficient increased with increasing condensing temperature. Further, for a given condensing temperature, the scraped film coefficient increased with mass flow rate (Fig. 4). At higher percentage solids at the outlet of SSHE the increasing condensing steam temperature had adverse effect on scraped film coefficient (Fig. 5). It was earlier mentioned that percent solids at the outlet was controlled by varying the mass flow rate of milk. When the mass flow rate was reduced to 1.80×10^{-2} kg/s the percentage solids at the outlet of SSHE was around 51%. The percentage solid increased to about 64% when the mass flow

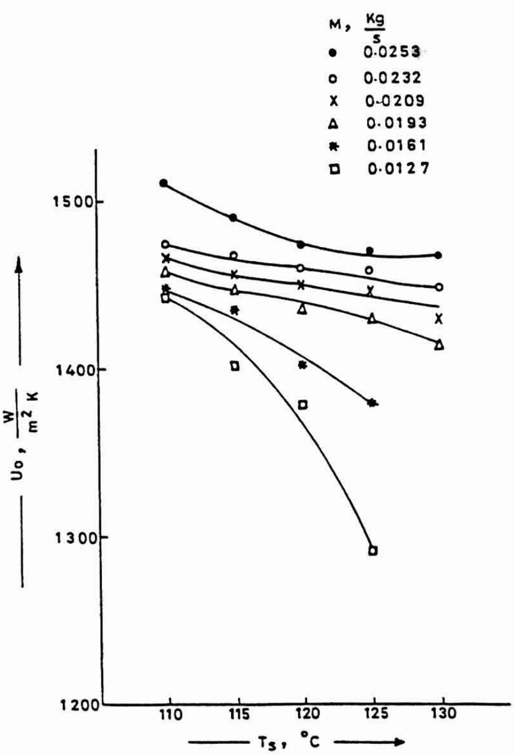

FIG. 3. EFFECT OF STEAM CONDENSING TEMPERATURE ON OVERALL HEAT TRANSFER COEFFICIENT

rate of milk was further reduced to 1.27×10^{-2} kg/s. In this range of concentration, the scraped film coefficient decreased with increasing condensing temperature.

It is of value to examine the reasons why h_s increases for certain total solids and then decreases. The blade clearance depends on the resultant of two forces, namely the centrifugal and hydrodynamic force (Bhattacharaya 1970). The hydrodynamic force (Fh) is defined as:

$$Fh = \frac{6\mu V_B}{(\text{Sin}\ \psi)^2}\left[\ \ln(1+C) - \frac{2C}{2+C}\right] L \tag{15}$$

The centrifugal force (F_c) is defined as:

$$F_c = 1/2\ (Mw^2h\ \text{Sin}\ \beta) \tag{16}$$

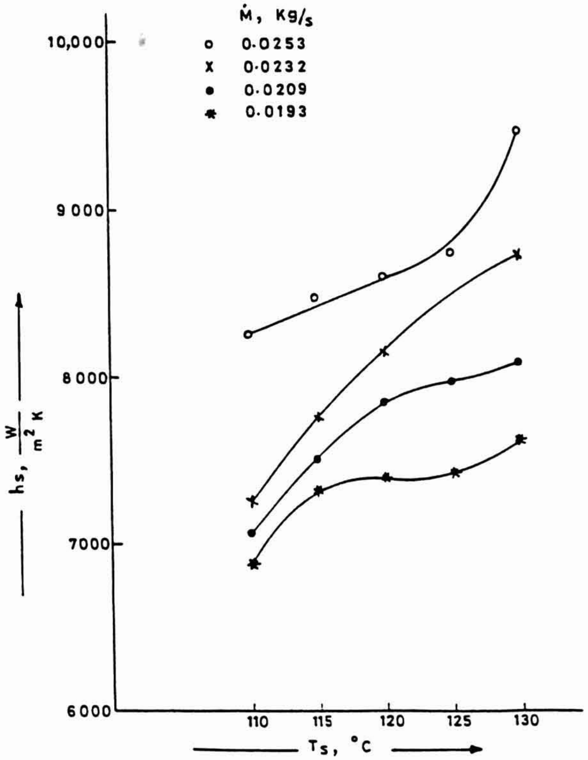

FIG. 4. EFFECT OF STEAM CONDENSING TEMPERATURE
ON SCRAPED FILM COEFFICIENT

At equilibrium Fh = Fc Sin ψ (17)

Where M = mass of agitator, g

V_B = linear velocity of blade tip, cm/sec

w = rotational speed of blades, radians/sec

μ = coefficient of viscosity

β = blade angle

ψ = angle between blade surface and normal at point of contact

L = length of blade, cm

h = length of spider arm, cm

δ = film thickness, cm

t = thickness of blade, cm

$$C = -\frac{t \sin \psi}{\mathrm{Cos}\,(\alpha + \psi)} \tag{18}$$

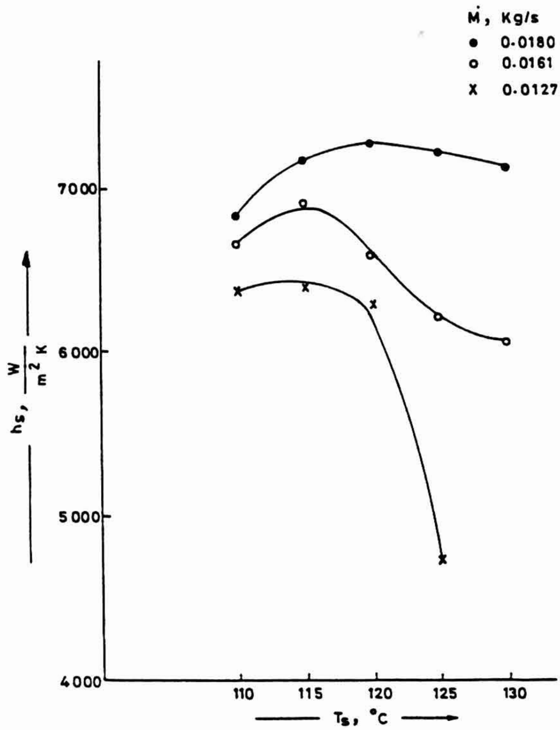

FIG. 5. EFFECT OF STEAM CONDENSING TEMPERATURE ON SCRAPED FILM COEFFICIENT

Thus, Eq. (15) gives the film thickness which is directly dependent on viscosity. Reinemann *et al.* (1973) have also shown a similar relationship.

Thus as long as viscosity effects are not predominant and with centrifugal force fixed (as all experiments are conducted at fixed rotor speed), the variation in film thickness may not be appreciable. Partly due to this reason and partly due to the fact that good mixing is possible between the fillet and scraped material from the film at low viscosities, higher evaporation is possible with increasing temperatures. As the scraped film coefficient increased with increasing temperature for mass flow rates from 1.93×10^{-2} kg/s to 2.53×10^{-2} kg/s. (this mass flow rates correspond to per cent outlet solids in the range of 19% to 45%), viscosity effects were not predominant until the product per cent solids was 45% at outlet.

It is evident from Fig. 4 that for a given condensing temperature, the scraped film coefficient increases with increasing mass flow rates or decreasing outlet solids. This should be so because the thermal conductivity of film increases with decreasing product outlet solids. Figure 6, which illustrates the variation of h_s with outlet per cent solids in milk further elucidates this point.

When the outlet solids in product increases beyond 45%, the scraped film coefficient begins to drop with condensing temperature as shown in Fig. 5. The outlet solids in product varied in this case from 51% to 64%. In this range of total solids, the viscosity of product would be much higher. For the reasons explained earlier, this would have caused film thickness to increase.

Equally important aspect is effect of diffusivity of water vapor in the product at the high concentration of solids. As concentration of solids increases the diffusivity of water would decrease rapidly. Fish (1958) measured the diffusion coefficient of water in starch gel etc. and found that it decreased by 1000 fold as the moisture content varied from 44% to 0.7%. Similar observations were made by Duckworth (1962). In general diffusivity of water in concentrated solutions was found to diminish rapidly with increasing solute concentrations (Loncin *et al.* 1979). Also, as viscosity increases, the diffusion coefficient must decrease considerably. Consequent to the effects of increasing viscosity of product resulting from evaporation, the diffusion coefficient of water in product would have dropped rapidly. This resultant effects of viscosity, thermal diffusivity and film thickness caused the evaporation rates to drop at higher total solids.

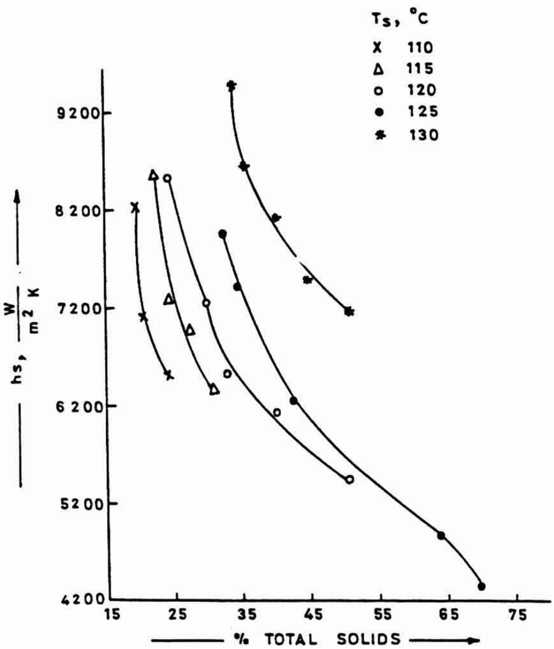

FIG. 6. EFFECT OF PERCENTAGE TOTAL SOLIDS IN PRODUCT ON SCRAPED FILM COEFFICIENT

It is thus established that while during concentration of milk up to 45% solids the scraped film coefficient increases with increasing steam condensing temperature, the drop in steam film coefficient had offset this effect to cause the overall heat transfer coefficient to decrease. Beyond 45% solids concentration, the effect of both scraped film coefficient and steam film coefficient were similar to decrease the overall heat transfer coefficient.

Thus, the value of overall heat transfer coefficient (U_o) decreased from 1511 $W/m^{2o}k$ (outlet solids 19.3%) to 1291 $W/m^{2o}k$ (outlet solids 64%). This establishes that thermal performance of thin film SSHE will not drop appreciably when milk is concentrated to higher percentage of solids. Undoubtedly such concentration would be difficult to attain in conventional evaporators without encountering problems of product fouling, browning etc.

CONCLUSION

Forty trials were conducted on heat transfer during evaporation of milk to high solids at various operating conditions. The correlation developed for predicting the scraped film heat transfer coefficient was found to be fairly accurate (correlation coefficient was 0.8492). The scraped film coefficient increased with increasing condensing temperature until the product attained about 45% solids. At higher concentrations beyond this level the scraped film coefficient decreased with increasing condensing temperature. This trend was due to increased viscosity and drop in diffusivity of water.

NOMENCLATURE

Ao	=	Outside area of heat exchanger, m^2
B	=	Number of blades
Cp	=	Specific heat kj/kg °K
Di	=	Inside diameter of heat exchanger, m
Do	=	Outside diameter of heat exchanger, m
hs	=	Scraped film heat transfer coefficient W/m^2ok
ho	=	Outside film heat transfer coefficient W/m^2ok
k	=	thermal conductivity of fluid, W/m^ok
km	=	Thermal conductivity at mean temperature W/m^ok
Lv	=	Latent heat of vaporization of water at atmospheric pressure
Mp	=	Mass flow rate of fluid, Kg/s
Mv	=	Evaporation rate, Kg/s
m	=	Flow behavior Index, $P_a{\cdot}s^n$
N	=	Rotor speed, rps

n	=	Consistency coefficient
Q	=	Total heat transferred, W
S	=	Percentage total solids, %
Ts	=	Temperature of condensing steam, °C
Tl	=	Saturation temperature of process fluid, °C
ΔT	=	Temperature difference °C
Uo	=	Overall heat transfer coefficient based on outside area of exchanger, W/m^2ok
V′	=	Velocity of fluid through exchanger, defined as volumetric flow per unit circumferential area of exchanger.
Vc	=	Circumferential velocity, m/s
ρ	=	density of fluid

DIMENSIONLESS GROUPS

$(NRe)_{Ge}$ = Generalized Reynolds number $\dfrac{D_i^n V'^{2-n}}{m\, 8^{n-1}}$

$(Pr)_{Ge}$ = Generalized Prandtl number $\dfrac{m\, C_p\, 8V^{n-1}}{k \quad D_i}$

REFERENCES

ABICHANDANI, H. and SARMA, S. C. Evaporation in a horizontal thin film scraped surface heat exchanger. J. Prod. Proc. Eng. (In press).

AGRAWALA, S. P. 1973. Studies on heat transfer characteristics of milk in falling film evaporator. Ph.D. Thesis, Dept. of Agri. Eng. IIT, Kharagpur.

ANGELL, C. W. and BAIRD, J. L. 1983. Rad Waste Volume reduction. Chem. Eng. Prog. (May), 52–55.

BHATTACHARYA, B. C. 1970. Design characteristics of a mechanically formed thin film evaporator. Chem. Proc. Equip. Sem. 1–6.

BRESSLER, R. Z. 1958. Ver. Deut., Ingrs. *100,* 257.

CHARM, S. F. and MERRILL, E. W. 1959. Heat transfer coefficient in straight tube for pseudoplastic food materials in streamline flow. Food Res. *24,* 319–331.

DUCKWORTH, R. B. 1962. *Recent Advances in Food Science,* Vol. 2, p. 46, Butterworth, London.

FERNANDEZ-MARTIN and MOHTES, F. 1972. Influence of temperature and composition on some physical properties of milk and milk concentrates. Milk. Sci. Int. *27,* 772–776.

FISH, B. P. 1958. Fundamental aspects of the dehydration of food stuffs. p. 143. Papers read at the conference held in Aberdeen, Society of Chemical Industry, London.
FREEZE, H. L. and GLOVER, W. B. 1979. Mechanically agitated thin film evaporator. Chem. Eng. Prog. (Jan) 52–58.
HARPER, J. C. 1960. Viscometric behavior in relation to evaporation of fruit juices. Food Technol. *14,* 557.
HAUSCHILD, W. 1969. Thin film evaporators/driers. Chem. Proc. Eng. *10,* 83.
HEADY, E. O. and DILLON, J. L. 1961. Forms of Production Functions. Agricultural Production Functions 1st ed. p. 75.
KESSLER, H. G. 1981. Food Eng. and Dairy Technology Verlag, p. 588. A. Kessler D-8050 Freising (F. R. Germany).
LONCIN, M. and MERSON, R. L. 1979. *Food Engineering,* p. 26. Academic Press, New York, San Francisco, London.
McADAMS, W. H. 1963. *Heat Transmission,* 3rd Ed. pp. 338–342. McGraw-Hill, Kogakusha Ltd.
REINEMANN, G., COMMEL, M. and DIETZ, H. 1973. Chem. Tech. *25,* 143.
SAWHNEY, I. K. and KUMAR, B. 1984. Characteristics of khoa at different stages of processing. J. Food Sci. Tech. *21*(6), 381–85.
SKOCZYLAS, A. 1970. Heat transfer coefficient for a hinged blade wiped film evaporator. Brit. Chem. Eng. *15*(2), 221–222.

MODELING THE AVERAGE SHEAR RATE IN A CO-ROTATING TWIN SCREW EXTRUDER

IBRAHIM O. MOHAMED,[1] ROBERT Y. OFOLI[2] and RON G. MORGAN[3]

Accepted for Publication January 10, 1990

ABSTRACT

A procedure similar to the one commonly used with mixers has been utilized to develop a model for estimating the shear rate in co-rotating twin screw extruders. Newtonian and non-Newtonian fluids were used to estimate the average shear rate for three screw configurations of a Baker Perkins (MPF-50D) twin screw extruder. As would be expected, the shear rate was highly correlated to the screw speed. At a given screw speed, 30 forwarding paddles generate the highest rate of shear, followed by feed screws and single lead screws. No data was found in the published literature to provide comparison with the results of this work. However, the model has performed well in heat transfer analysis of twin screw processes.

The procedure is sensitive to screw configuration, accounts for the shearing effects in the different regions within the extruder barrel, and covers a range of screw speeds (100–400 RPM) typical of what is encountered in industrial pilot plants. Even though much more work remains to be done before the shear rate can be confidently characterized for composite screw configurations, this technique provides a sound foundation.

INTRODUCTION

The shear rate is critical in evaluating viscous dissipation, which constitutes the major source of heat energy for cooking extruders. The approach generally used for calculating the shear rate in twin screw extruders is similar to the one used with single screw extruders, for which the shear rate is calculated as the ratio of the screw tip velocity to the channel or clearance depth (Martelli 1971; Yacu 1985; Meijer and Eleman 1988).

The drawback of this approach is that, due to geometric complexity, it is difficult to accurately quantify the shear rate at the different shearing zones of

[1]University of Gezira, Wad Medani, Sudan.
[2]All correspondence to: Dr. Robert Y. Ofoli, 205 A. W. Farrall Hall, Michigan State University, East Lansing, Michigan 48824–1323.
[3]Kraft, Inc., Glenview, Illinois.

the twin screw extruder. In addition, the generally good mixing which occurs in twin screw extruders disrupts the velocity profile, and raises questions about the applicability of the single screw method. The capability to promote mixing, however, suggests that a mixer approach might be more appropriate for modeling the shear rate in extruders.

The objective of this paper is to present and evaluate a procedure for estimating the average shear rate in co-rotating twin screw extruders.

THEORETICAL DEVELOPMENT

The power consumption in mixing vessels is usually expressed in terms of a dimensionless power number which, for twin screw extruders, may be characterized as

$$P_o = \frac{E_v}{\rho N^3 D_h^5} \tag{1}$$

The power consumed in mixing a Newtonian fluid in the laminar region is inversely proportional to the Reynolds number (Metzner and Otto 1957; Rieger and Novak 1973). The Reynolds number for a Newtonian fluid in a twin screw extruder may be defined as

$$Re = \frac{D_h^2 N \rho}{\mu} \tag{2}$$

To use Eq. 1 and 2, two quantities must be known: the characteristic diameter of the extruder, and the rate of viscous dissipation of mechanical energy in the extruder.

Characteristic diameter of the extruder

Since the barrel diameter is independent of screw configuration, it is not a useful characteristic dimension for twin screw extruders. However, the hydraulic diameter, which has been used extensively to characterize the geometry of complex shapes, provides a meaningful dimension. In particular, because its calculation uses dimensions of the screw as well as the barrel, it ensures that the screw configuration is accounted for.

The expression below

$$D_h = \frac{4\,V_w}{A_w} \tag{3}$$

was used to calculate the hydraulic diameter of each of the three screws used in this study. The procedures are summarized below.

Single Lead Screws. The profile of a typical twin screw extruder is shown in Fig. 1. To calculate the hydraulic diameter for single lead screws, a 5.08 cm (2-inch) screw length was chosen as a basis. The wetted volume was estimated by

$$V_w = V_b - 2V_s \tag{4}$$

The barrel volume was calculated by

$$V_b = A_{bc}L \tag{5}$$

where

$$A_{bc} = \frac{1}{2}(\pi - \psi)D^2 + \frac{C_L D}{2}\sin\psi \tag{6}$$

The volume of the screw, V_s was estimated by sealing both ends of the screw and using a beaker to determine the volume of water displaced, which is equivalent to the screw volume.

The wetted surface area was estimated by

$$A_w = A_{bs} + 2A_s \tag{7}$$

where

$$A_{bs} = P_{bp}L = 2D(\pi - \psi)L \tag{8}$$

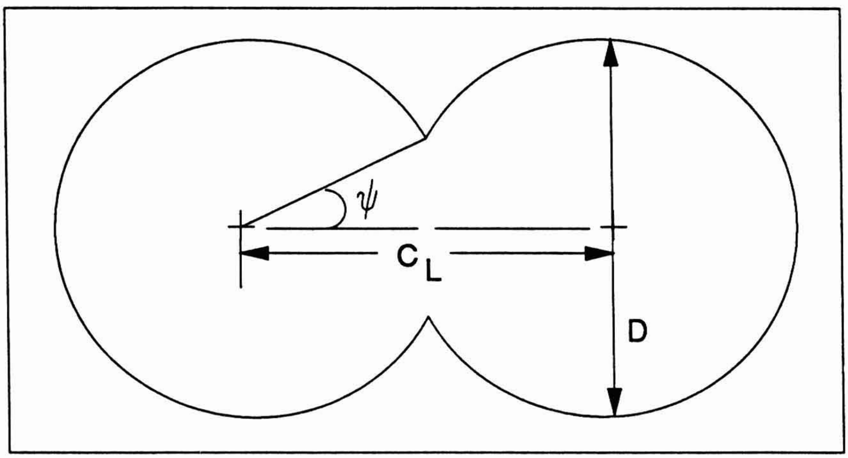

FIG. 1. BARREL CROSS-SECTION OF TWIN SCREW EXTRUDER

and

$$A_s = Z_t e + Z_r W + 2H Z_t \tag{9}$$

Feed Screws. The wetted volume was estimated in a manner similar to the single lead. The screw surface area was estimated by combing the flange and root areas. Since the screw has a parabolic shape, the flange and root areas are related by

$$A_r + A_f = 2B Z_t \tag{10}$$

The tip area is given by

$$A_t = 2Z_t e \tag{11}$$

30 Degree Forwarding (30F) paddles. A procedure similar to the one used with the single lead and feed screws was used to estimate the wetted volume. The wetted area for kneading discs staggered at 30 degree forwarding (30F) consists of the tip area, side area and flange area. The tip and side areas were determined from routine measurements. The flange area was obtained by drawing the discs with the staggered angle to scale, and estimating the wetted area.

For a barrel length of 5.08 cm and disc width of 1.27 cm, four discs are required per shaft. This adds up to three flange areas and four tip and side areas. Therefore the total disc surface area is given by

$$A_s = 2(3A_f + 4A_t + 4A_{ds}) \tag{12}$$

Viscous Energy Dissipation of Mechanical Energy

The energy provided by the extruder shaft may be distributed among two primary functions: viscous dissipation and the production of a net flow out of the extruder. Since the net flow is the difference between drag flow and back flow due to pressure at the die, one can represent the total energy consumption in the extruder by

$$P_w = E_v + \Delta P\, Q_n \tag{13}$$

from which the contribution due to viscous dissipation may be obtained as

$$E_v = P_w - \Delta P\, Q_n \tag{14}$$

Shear Rate Modelling

The strategy used to calculate the average shear rate is analogous to the method suggested by Metzner and Otto (1957) for commercial mixers, and recently used in mixer viscometry (Mackey *et al.* 1987). It is also based on the following premise, presented by Rao and Cooley (1984), regarding two identical mixing systems (one containing a Newtonian and the other a non-Newtonian fluid) operating in the laminar region with identical impeller speeds: if the viscosity of the Newtonian fluid is varied by diluting or thickening until the power measured on each mixer is the same, then the apparent viscosity of the non-Newtonian fluid must be the same as the viscosity of the Newtonian fluid.

The average rather than the true shear rate is used in this exercise because the apparent viscosity varies with shear rate for non-Newtonian fluids. The apparent viscosity at this shear rate will be characterized the "average apparent viscosity" and assumed to be equivalent to the Newtonian viscosity at the same power number and screw speed.

The following steps can be used to calculate the average shear rate:

(1) From data collected during the extrusion of the Newtonian fluid, calculate the power number (P_o) and Reynolds number (Re), using Eq. (1) and (2).
(2) Obtain an equation correlating P_o and Re.
(3) From data collected during the extrusion of the non-Newtonian fluid, calculate the power number using Eq. (1).
(4) Use P_o from step 3 and the correlation from step 2 to calculate the corresponding Reynolds number.
(5) Use the Reynolds number from step 4 and Eq. (2) to calculate the viscosity of the fluid. This viscosity, in effect, is the average apparent viscosity (η) for the non-Newtonian fluid.
(6) Use an appropriate rheological instrument to obtain the shear rate dependence of the non-Newtonian fluid.
(7) From the average apparent viscosity (η) and the rheological equation of step 6, calculate the corresponding average shear rate ($\dot{\gamma}_a$).
(8) Correlate the average shear rate ($\dot{\gamma}_a$) to screw speed and throughput.

MATERIALS AND METHODS

Newtonian and non-Newtonian standards were used to obtain the data needed to estimate the effective shear rate. Polybutene (Amoco) was chosen as the Newtonian standard, because of its high viscosity and availability in melt form at room temperature. The non-Newtonian standard was prepared by mixing seven parts soy polysaccharide (SPS) with 93 parts pure honey. The sample was left overnight to allow air bubbles to settle out before extrusion.

Rheological Data

A Haake concentric cylinder viscometer (M-150 measuring head; SV I and SV II sensors) was used to determine rheological properties. The viscometer was connected to a Haake speed programmer, a Hewlett-Packard 3495 data acquisition system, and a Hewlett-Packard 85 computer to facilitate data collection and analysis. A Haake F3-C temperature controller was used to control fluid temperature.

The samples used to determine the rheological properties, for both the Newtonian and the non-Newtonian fluids, were taken from the same batch used for the extrusion runs. Data for both fluids were taken at different temperatures over as wide a shear rate range as possible.

Twin Screw Extrusion Data

A Baker Perkins (MPF-50D) co-rotating twin screw extruder was used. All extrusion runs were performed over 15 L/D, using a configuration of one type of screw at a time. A special die with a gate valve was constructed and used in all the extrusion runs to control die pressure and degree of fill. A K-tron feeder (K-tron Corporation) with a controllable auger speed was used to feed the material into the extruder.

During extrusion, the barrel temperature was controlled by circulating chilled water to maintain low product temperatures and high torque readings. A major objective was to maintain 100% fill levels. This was achieved by manipulating the feed rate and die pressure until the channel was filled, which was monitored by observing the material back up to the feed port. When 100% fill was achieved, the extruder was allowed to equilibrate before making any measurements. Screw speed, torque, barrel temperature, product temperature and die pressure were recorded at the controller panel. Flow rates were obtained by measuring extrudate weight over a given time span. The product temperature at the die was measured by inserting a thermocouple through the die opening. Measurements were made for all three screw configurations on both the Newtonian and non-Newtonian fluids.

RESULTS

Physical Constants

Geometric information and results of volume and surface area calculations are presented in Tables 1, 2 and 3, as well as the calculated values of the hydraulic diameters of the three screws.

TABLE 1.
DIMENSIONS OF SINGLE LEAD SCREW AND EXTRUDER BARREL*

Variable	Symbol	Value
Major diameter	(D_s)	50.2 mm
Root diameter	(D_r)	28.6 mm
Channel depth	(H)	11.1 mm
Tip width	(e)	2.6 mm
Channel bottom width	(E)	5.3 mm
Distance between screw shafts	(C_L)	40.0 mm
Helix angle	ϕ	4.6°
Length of tip along helix	Z_t	633.4 mm*
Length of root along helix	Z_r	342.4 mm*
Tip area	A_t	16.7 cm^2
Root area	A_r	18.0 cm^2
Flange area	A_f	140.6 cm^2
Volume	V_s	51.5 cm^3
Angle shown in Figure 1	ψ	38.0°
Barrel diameter	(D)	50.8 mm
Barrel volume	V_b	193.2 cm^3
Barrel surface area	A_{bs}	127.8 cm^2
Wetted volume	V_w	90.2 cm^3
Wetted area	A_w	478.6 cm^2
Hydraulic diameter	D_h	0.75 cm

*Volume and surface area are based on a 5.08 cm (2-inch) axial length

Rheological Properties

Newtonian Standard. The shear stress versus shear rate data for polybutene are presented in Fig. 2 at temperatures of 40, 60 and 80°C. The plots indicate clearly that polybutene is Newtonian. Also a regression analysis of the data gave a power index (flow behavior index) of 1, based on the power law model. The rheological properties are summarized in Table 4. Temperature effects were incorporated into the consistency coefficient (which for Newtonian fluids, is the same as the viscosity) by an Arrhenius expression:

$$\mu = K(T) = K_o e^{\left(\frac{\Delta E}{RT}\right)} \tag{15}$$

A plot of log μ versus the reciprocal temperature gave an activation energy of 12995 cal/g mole.

TABLE 2.
DIMENSIONS OF FEED SCREW

Variable	Symbol	Value
Major diameter	(D_s)	50.2 mm
Root diameter	(D_r)	29.6 mm
Channel depth	(H)	10.4 mm
Tip width	(e)	1.5 mm
Helix angle	ϕ	17.8°
Length of tip along helix	Z_t	165.8 mm*
Root and flange area	A_r+A_f	105.6 cm^3
Screw tip area	A_t	4.9 cm^2
Volume	V_s	52.4 cm^3
Screw root area	A_r	18.0 cm^2
Wetted volume	V_w	88.4 cm^3
Wetted area	A_w	348.9 cm^2
Hydraulic diameter	D_h	1.01 cm

*Volume and surface area are based on a 5.08 cm (2-inch) axial length

Non-Newtonian fluid. A plot of shear stress versus shear rate for the honey/SPS system is shown in Fig. 3. Regression analysis of the data gave a power law fit (Table 4). Again, the consistency coefficient was used to reflect the temperature effects on the viscosity:

$$\eta = K(T)\dot{\gamma}^{n-1} = K_o e^{\left(\frac{\Delta E}{RT}\right)}\dot{\gamma}^{n-1} \tag{16}$$

TABLE 3.
DIMENSION OF 30F PADDLES*

Variable	Symbol	Value
Disc volume	V_s	14.0 cm^3
Wetted volume	V_w	81.2 cm^3
Disc tip area	A_t	1.3 cm^2
Disc flange area	A_f	1.9 cm^2
Disc side area	A_{ds}	14.5 cm^2
Wetted area	A_w	265.3 cm^2
Hydraulic diameter	D_h	1.22 cm

*All measurements are based on a 5.08 cm (2-inch) axial length

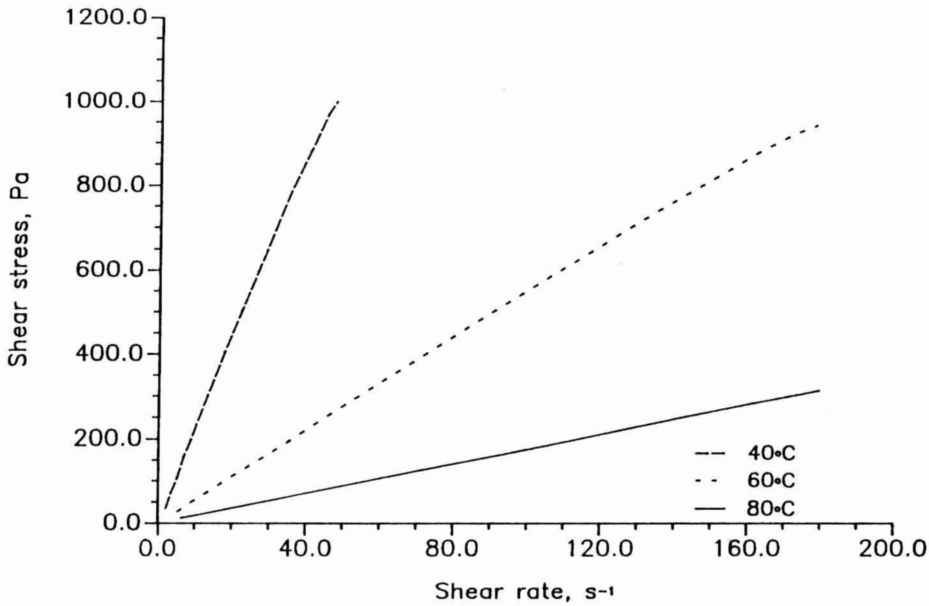

FIG. 2. SHEAR STRESS VERSUS SHEAR RATE FOR POLYBUTENE

TABLE 4.
RHEOLOGICAL PROPERTIES OF EXPERIMENTAL FLUIDS

Newtonian standard (polybutene)

Temperature	K (Pa s^n)	n	R^2
40	19.31	1.03	0.99
60	5.44	1.00	1.00
80	1.80	0.99	1.00

Non-Newtonian fluid (7% SPS and 93% honey)

Temperature	K (Pa s^n)	n	R^2
40	172.61	0.422	0.98
60	93.07	0.425	0.97
80	50.88	0.402	0.97

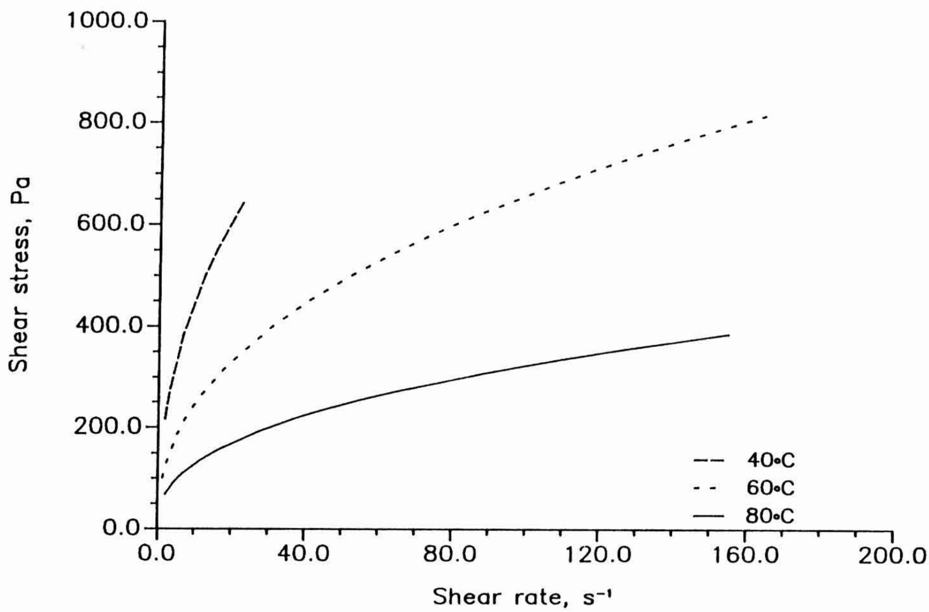

FIG. 3. SHEAR STRESS VERSUS SHEAR RATE OF 7% SPS AND 93% HONEY

A plot of log K versus the reciprocal temperature gave an activation energy of 7904 cal/g mole.

Estimation Of The Average Shear Rate

The dimensionless power number was calculated on the basis of the power used to shear the material. The total power input to the extruder was calculated from the torque reading, using the manufacturer's correlation:

$$P_w = 0.354\,(\%\ torque)\,N \tag{17}$$

Equations 1, 14 and 17 were used to calculate the power number. The Reynolds number was calculated by Eq. 2, with the viscosity evaluated at the average of the temperature of the product at the inlet and outlet of the extruder. Plots of power number versus Reynolds number for the three screw configurations are shown in Fig. 4, based on the Newtonian data.

In mixing systems, the plot of log (P_o) versus log (Re) usually yields a slope of approximately one. In twin screw extruders, because there is conveying as well as mixing, the following general model is proposed for correlating the power number to the Reynolds number

$$P_o = \frac{\beta}{Re^{\lambda}} \tag{18}$$

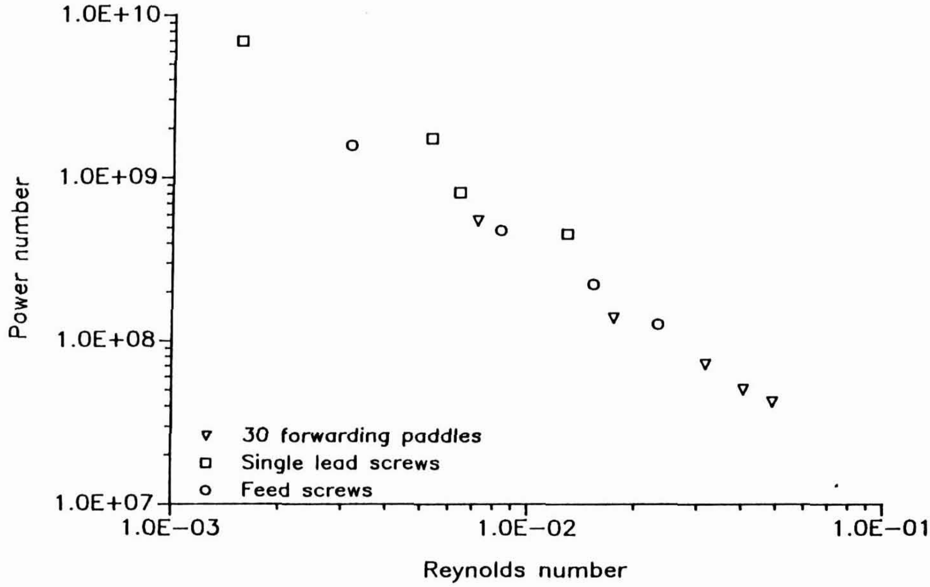

FIG. 4. POWER NUMBER VERSUS REYNOLDS NUMBER FOR POLYBUTENE

where β and λ are constants which depend on the screw configuration.

Equation 18 was transformed to

$$\log P_o = \log \beta + \lambda \log Re \tag{19}$$

to enable the variables β and λ to be evaluated by linear regression. The results of the regression are shown in Table 5, and portray an excellent fit. It is worth noting that the proportionality between P_o and Re shown here is the same as observed for mixers. However, the parameter λ is usually unity for mixers.

The power number was also calculated for the non-Newtonian fluid for each of the three screw configurations, based on the correlation developed for the Newtonian fluid. The Reynolds number was used to calculate the equivalent apparent viscosity for the non-Newtonian fluid by

$$\eta_a = \frac{\rho_n D_h^2 N}{Re^*} \tag{20}$$

TABLE 5.
RESULTS OF REGRESSION ANALYSIS OF EQUATION 19.

Screw	log β	λ	R^2
Single lead	6.15	-1.31	0.97
Feed screw	6.04	-1.26	0.98
30° forwarding	5.84	-1.34	0.98

where Re* is the equivalent non-Newtonian Reynolds number.

Then, using the apparent viscosity correlation developed from rheometry, the average shear rate can be found from

$$\dot{\gamma}_a = \left[\eta\left(K_o \exp\left(\frac{\Delta E}{RT_a}\right)\right)^{-1}\right]^{1/(n-1)} \tag{21}$$

where T_a is the average product temperature.

Table 6 shows the calculated values of the average shear rate for the three screw configurations. The average shear rate for the kneading discs is the highest,

TABLE 6.
AVERAGE SHEAR RATES FOR THREE SCREW CONFIGURATIONS

a) Single Lead Screws

Screw speed (RPM)	$\dot{M}$ (kg s^{-1})	$\dot{\gamma}_a$ (s^{-1})
100	0.0150	23.4
150	0.0243	28.8
200	0.0227	33.0
300	0.0201	36.6
400	0.0268	42.5

b) Feed Screws

Screw speed (RPM)	$\dot{M}$ (kg s^{-1})	$\dot{\gamma}_a$ (s^{-1})
100	0.0216	35.3
200	0.0237	56.1
250	0.0473	64.2
300	0.0308	67.8
400	0.0384	72.5

c) 30F Paddles

Screw speed (RPM)	$\dot{M}$ (kg s^{-1})	$\dot{\gamma}_a$ (s^{-1})
100	0.0189	53.3
150	0.0069	62.1
200	0.0242	79.8
300	0.0302	85.8
400	0.0464	99.1

followed by feed screws and single lead screws, as would be expected. There is no published data on the shear rate of twin screw extruders for comparison. However, these values are of the same order of magnitude as the shear rate data of Rossen and Miller (1973) for single screw extruders. Eise *et al.* (1982) and Altomare and Ghossi (1986) have shown that screw speed and throughput are the primary variables affecting the shear rate in twin-screw extruders. The following models are, therefore, proposed for correlating the average shear rate in twin screw extruders

$$\dot{\gamma}_a = \alpha_1 N^{\alpha_2} \tag{22}$$

$$\dot{\gamma}_a = \beta_1 N^{\beta_2} \dot{M}^{\beta_3} \tag{23}$$

where α_1, α_2, β_1, β_2 and β_3 are constants which depend on the screw configuration.

The non-linear equations above were transformed to the forms below, to convert the problem to one of linear parameter estimation.

TABLE 7.
RESULTS OF REGRESSION OF PARAMETERS
IN EQS. 24 AND 25 FOR SINGLE LEAD SCREWS.

Equation 24:

Parameter	Estimated value	Estimated standard error	t
$\log \alpha_1$	1.288	0.0162	79.6
α_2	0.413	0.0281	14.7

Standard error = 1.34E-2 $R^2 = 0.986$

Equation 25:

Parameter	Estimated value	Estimated standard error	t
$\log \beta_1$	1.540	0.106	14.5
β_2	0.374	0.0248	15.1
β_3	0.138	0.0580	2.4*

Standard error = 9.03E-3 $R^2 = 0.996$

*Test of significance of β_3: The term must be included if $t > 3.182$.

$$\log \dot{\gamma}_a = \log \alpha_1 + \alpha_2 \log N \tag{24}$$

$$\log \dot{\gamma}_a = \log \beta_1 + \beta_2 \log N + \beta_3 \log \dot{M} \tag{25}$$

A computer program developed by Beck (1978) was modified and used to estimate the parameters in Eq. 24 and 25, using least squares based on the sequential parameter estimation method (Beck and Arnold 1977). The results of the regression analysis are presented in Tables 7, 8 and 9 for single lead screws, feed screws, and 30F paddles, respectively. The results show that both Eq. 24 and 25 fit the data accurately for all three screw configurations, with slight differences in the error sum of squares.

A student t-test was performed to determine if inclusion of the flow rate term in Eq. 25 is significant, using t (0.975,3) = 3.182 as the test of significance. The results for all three screw configurations suggested that setting $\beta_3 = 0$ does not significantly affect the accuracy of predictions.

TABLE 8.
RESULTS OF REGRESSION OF PARAMETERS IN EQS. 24 AND 25 FOR FEED SCREWS.

Equation 24:

Parameter	Estimated value	Estimated standard error	t
$\log \alpha_1$	1.448	0.0384	37.7
α_2	0.539	0.0627	8.6

Standard error = 2.86E-2 $R^2 = 0.961$

Equation 25:

Parameter	Estimated value	Estimated standard error	t
$\log \beta_1$	1.564	0.290	5.4
β_2	0.510	0.103	4.9
β_3	0.066	0.016	0.4*

Standard error = 3.38E-2 $R^2 = 0.963$

*Test of significance of β_3: The term must be included if t > 3.182.

TABLE 9.
RESULTS OF REGRESSION OF PARAMETERS IN EQS. 24 AND 25 FOR 30F PADDLES.

Equation 24:

Parameter	Estimated value	Estimated standard error	t
$\log \alpha_1$	1.631	0.0290	56.1
α_2	0.448	0.0506	8.5

Standard error = 2.42E-2 $R^2 = 0.963$

Equation 25:

Parameter	Estimated value	Estimated standard error	t
$\log \beta_1$	1.710	0.135	12.7
β_2	0.414	0.0790	5.2
β_3	0.035	0.0061	0.6*

Standard error = 2.73E-2 $R^2 = 0.968$

*Test of significance of β_3: The term must be included if t > 3.182.

The final equations are:

Single lead screws:

$$\dot{\gamma}_a = 19.4\, N^{0.413} \tag{26}$$

Feed screws:

$$\dot{\gamma}_a = 28.0\, N^{0.539} \tag{27}$$

30F paddles:

$$\dot{\gamma}_a = 42.8\, N^{0.448} \tag{28}$$

Table 10 shows the residuals and percent error from using Eq. 26, 27 and 28 to estimate the shear rate. The maximum absolute error is 8%.

TABLE 10.
OBSERVED VERSUS PREDICTED AVERAGE SHEAR RATES

a) Single Lead Screws

N, RPM	Observed Shear Rate, s^{-1}	Predicted Shear Rate, s^{-1}	% Error
100	23.4	23.9	-2.1
150	28.8	28.3	1.7
200	33.0	31.9	3.3
300	36.6	37.7	-3.0
400	42.5	42.4	0.2

b) Feed screws

N, RPM	Observed Shear Rate, s^{-1}	Predicted Shear Rate, s^{-1}	% Error
100	35.3	36.9	-4.5
200	56.1	53.7	4.3
250	64.2	60.5	5.8
300	67.8	66.8	1.5
400	72.5	78.0	-7.6

c) 30F paddles

N, RPM	Observed Shear Rate, s^{-1}	Predicted Shear Rate, s^{-1}	% Error
100	53.3	53.8	-0.9
150	62.1	64.5	3.9
200	79.8	73.4	8.0
300	85.5	88.0	-2.6
400	99.1	100.1	-1.0

DISCUSSION

It is fully anticipated that this paper will answer several questions and leave many others unanswered, since there are several important aspects of extruders and screw configurations that could not be accommodated in this study. For example, since all experiments were conducted under conditions of fully-filled screws and most twin-screw extruders run at partially-filled levels in normal modes of operation, it is reasonable to inquire as to the validity of this technique in practical situations.

Partially-filled screws do present a problem in characterizing the shear rate, particularly with respect to the calculation of the hydraulic diameter since it is difficult to characterize the wetted area. However, there is some evidence from recent experiments to indicate that the method presented in this paper would be useful in characterizing the average shear rate in twin screw extruders for partially-filled screws (Komolprasert 1989). This would require the determination of a residence time distribution, from which an equivalent flow path and an approximate cross-sectional area can be calculated to be used in estimating the hydraulic diameter.

Secondly, since only a constant screw configuration and one pair of dies were used in this study, it would be of interest to assess the effects of varying screw configurations and die geometry. As is well known, the screw configuration affects the pitch, flight height to channel width ratio, pressure and velocity profiles, etc. In addition, both the length and cross-sectional area of the extruder die affect pressure and velocity profiles and, therefore, also affect the shear rate. Again, some recent work (Komolprasert 1989) using nonhomogeneous screw configurations suggests that this method is valid if the hydraulic diameter is calculated in terms of the composite screw configuration.

The position of the authors is that the significance of this paper lies not so much in the absolute results or the shear rate correlations presented, but rather in the systematic procedure outlined for estimating the shear rate in a twin screw extruder. It is hoped that there would be several follow-up studies to help provide answers to the important questions raised above.

CONCLUSIONS

A procedure has been developed and presented for estimating the average shear rate for twin screw extruders. At a given screw speed, the 30 forwarding paddles generate the highest shear rate followed by feed screws and single lead screws. No data was found in the published literature to provide comparison with the results of this work. However, the model has performed well in heat transfer analysis of twin screw processes (Mohamed 1988).

The average shear rate obtained by this procedure is a weighted value. Since the procedure is sensitive to screw configuration, the shearing effects from the different regions within the extruder barrel are accounted for. Data were collected over a range of screw speeds (100–400 RPM) typical of what is encountered in industrial pilot plants. While much remains to be done before the shear rate can be confidently characterized in composite screw configurations, this technique provides a sound foundation for modeling.

NOMENCLATURE

A_{bc}	barrel cross-sectional area, m^2
A_{bs}	barrel surface area, m^2
A_{ds}	kneading disc side area, m^2
A_f	screw flange area, m^2
A_r	screw root area, m^2
A_s	screw surface area, m^2
A_t	screw tip area, cm^2
A_w	wetted area, m^2
B	perimeter of feed screw channel perimeter, m
C_L	dimension defined in Fig. 1.
D	barrel diameter, m
D_h	hydraulic diameter, m
e	screw tip width, m
E	screw channel bottom width, m
E_v	viscous dissipation of mechanical energy, W
H	channel depth, m
K	consistency coefficient, Pa s
K_o	reference consistency coefficient, Pa s
L	barrel length, m
n	flow behavior index, dimensionless
N	screw speed, RPS
P_o	power number, dimensionless
P_o^*	power number of non-Newtonian fluids, dimensionless
P_{bp}	barrel perimeter, cm
P_w	total power input to extruder (shaft work), W
Q_d	drag flow rate, m^3h^{-1}
Q_n	net flow rate, m^3h^{-1}
Q_p	pressure flow rate, m^3h^{-1}
R	gas constant, cal (gm-mole°K)$^{-1}$
Re	Reynolds number
Re^*	equivalent non-Newtonian Reynolds number
T	temperature, °C
T_o	reference temperature, °C
V_b	barrel volume, m^3
V_s	screw volume, m^3
V_w	wetted volume, m^3

W width of screw root, m
Z_t length of tip along screw helix, m
Z_r length of root along screw helix, m

GREEK SYMBOLS

α_1 constant (Eq. 22)
α_2 constant (Eq. 22)
β constant (Eq. 18)
β_1 constant (Eq. 23)
β_2 constant (Eq. 23)
β_3 constant (Eq. 23)
$\triangle E$ activation energy, cal (g mole)$^{-1}$
$\triangle P$ pressure drop across extruder, Pa
ρ Newtonian fluid density, kg m^{-3}
ρ_n non-Newtonian fluid density, kg m^{-3}
η non-Newtonian apparent viscosity, Pa s
$\dot{\gamma}$ shear rate, s^{-1}
$\dot{\gamma}_a$ average shear rate, s^{-1}
λ constant (Eq. 18)
ψ angle shown in Fig. 1
ϕ screw helix angle
μ Newtonian viscosity, Pa s

REFERENCES

ALTOMARE, E. and GHOSSI, P. 1986. Analysis of residence time distribution pattern in a twin screw cooking extruder. *Biotech. Prog. 2*(3), 157–163.

BECK, J. V. 1978. NONLINBG. Unpublished computer program, Dept. Mech. Eng., Mich. State Univ., East Lansing, Michigan.

BECK, J. V. and ARNOLD, K. J. 1977. *Parameter Estimation in Engineering and Science,* John Wiley & Sons, New York.

EISE, K., HERRMANN, H., JAKOPIN, S. and BURKHARDT, U. 1981. An analysis of twin-screw extruder mechanisms. *Adv. Plastic Technol. 2*(1), 18–39.

KOMOLPRASERT, V. 1989. *Starch liquefaction by thermostable alpha-amylase during reactive extrusion.* Ph.D. Dissertation, Mich. State Univ., East Lansing, Michigan.

MARTELLI, F. G. 1971. Twin-screw extruders—a separate breed. *SPE. J. 27*(1)P, 25–30.

MACKEY, K. L., MORGAN, R. G. and STEFFE, J. F. 1987. Effects of shear-thinning behavior on mixer viscometry techniques. *J. Texture Studies 18*(3), 23–240.

MARTELLI, F. G. 1983. *Twin screw Extruders: A Basic Understanding*, Van Nostrand Reinhold, New York.

MEIJER, H. E. H. and ELEMAN, P. H. M. 1988. The modelling of a continuous mixer. Part 1: The co-rotating twin-screw extruder. *Polym. Eng. Sci 28*(5), 275–290.

METZNER, A. B. and OTTO, R. E. 1957. Agitation of non-Newtonian fluids. *AIChE J. 3*(1), 3–10.

MOHAMED, I. O. 1988. *Modelling shear rate and heat transfer in a co-rotating food extruder*. Ph.D. Dissertation, Mich. State Univ., East Lansing, Michigan.

RAO, M. A. and COOLEY, H. J. 1984. Determination of effective shear rates in rotating viscometers with complex geometry. *J. Texture Studies 15*, 327–335.

RIEGER, F. and NOVAK, V. 1973. Power consumption of agitators in highly viscous non-Newtonian liquids. *Trans. Instn. Chem. Engrs. 51*, 105–111.

ROSSEN, J. L. and MILLER, R. C. 1973. Food extrusion. *Food Technol. 27*, 46–53.

YACU, W. 1985. Modelling a twin screw co-rotating extruder. *J. Food Proc. Eng. 8*, 1–21.

F
N
P

PUBLICATIONS IN FOOD SCIENCE AND NUTRITION

Journals

JOURNAL OF MUSCLE FOODS, N.G. Marriott and G.J. Flick, Jr.
JOURNAL OF SENSORY STUDIES, M.C. Gacula, Jr.
JOURNAL OF FOOD SERVICE SYSTEMS, O.P. Snyder, Jr.
JOURNAL OF FOOD BIOCHEMISTRY, J.R. Whitaker, N.F. Haard and H. Swaisgood
JOURNAL OF FOOD PROCESS ENGINEERING, D.R. Heldman and R.P. Singh
JOURNAL OF FOOD PROCESSING AND PRESERVATION, D.B. Lund
JOURNAL OF FOOD QUALITY, R.L. Shewfelt
JOURNAL OF FOOD SAFETY, T.J. Montville and A.J. Miller
JOURNAL OF TEXTURE STUDIES, M.C. Bourne and P. Sherman

Books

CONTROLLED/MODIFIED ATMOSPHERE/VACUUM PACKAGING OF FOODS, A.L. Brody
NUTRITIONAL STATUS ASSESSMENT OF THE INDIVIDUAL, G.E. Livingston
QUALITY ASSURANCE OF FOODS, J.E. Stauffer
THE SCIENCE OF MEAT AND MEAT PRODUCTS, 3RD ED., J.F. Price and B.S. Schweigert
HANDBOOK OF FOOD COLORANT PATENTS, F.J. Francis
ROLE OF CHEMISTRY IN THE QUALITY OF PROCESSED FOODS, O.R. Fennema, W.H. Chang and C.Y. Lii
NEW DIRECTIONS FOR PRODUCT TESTING AND SENSORY ANALYSIS OF FOODS, H.R. Moskowitz
PRODUCT TESTING AND SENSORY EVALUATION OF FOODS, H.R. Moskowitz
ENVIRONMENTAL ASPECTS OF CANCER: ROLE OF MACRO AND MICRO COMPONENTS OF FOODS, E.L. Wynder *et al.*
FOOD PRODUCT DEVELOPMENT IN IMPLEMENTING DIETARY GUIDELINES, G.E. Livingston, R.J. Moshy, and C.M. Chang
SHELF-LIFE DATING OF FOODS, T.P. Labuza
RECENT ADVANCES IN OBESITY RESEARCH, VOL. V, E. Berry, S.H. Blondheim, H.E. Eliahou and E. Shafrir
RECENT ADVANCES IN OBESITY RESEARCH, VOL. IV, J. Hirsch *et al.*
RECENT ADVANCES IN OBESITY RESEARCH, VOL. III, P. Bjorntorp *et al.*
RECENT ADVANCES IN OBESITY RESEARCH, VOL. II, G.A. Bray
RECENT ADVANCES IN OBESITY RESEARCH, VOL. I, A.N. Howard
ANTINUTRIENTS AND NATURAL TOXICANTS IN FOOD, R.L. Ory
UTILIZATION OF PROTEIN RESOURCES, D.W. Stanley *et al.*
FOOD INDUSTRY ENERGY ALTERNATIVES, R.P. Ouellette *et al.*
VITAMIN B_6: METABOLISM AND ROLE IN GROWTH, G.P. Tryfiates
HUMAN NUTRITION, 3RD ED., F.R. Mottram
FOOD POISONING AND FOOD HYGIENE, 4TH ED., B.C. Hobbs *et al.*
POSTHARVEST BIOLOGY AND BIOTECHNOLOGY, H.O. Hultin and M. Milner

Newsletters

FOOD INDUSTRY REPORT, G.C. Melson
FOOD, NUTRITION AND HEALTH, P.A. Lachance and M.C. Fisher
FOOD PACKAGING AND LABELING, S. Sacharow

GUIDE FOR AUTHORS

Typewritten manuscripts in triplicate should be submitted to the editorial office. The typing should be double-spaced throughout with one-inch margins on all sides.

Page one should contain: the title, which should be concise and informative; the complete name(s) of the author(s); affiliation of the author(s); a running title of 40 characters or less; and the name and mail address to whom correspondence should be sent.

Page two should contain an abstract of not more than 150 words. This abstract should be intelligible by itself.

The main text should begin on page three and will ordinarily have the following arrangement:

Introduction: This should be brief and state the reason for the work in relation to the field. It should indicate what new contribution is made by the work described.

Materials and Methods: Enough information should be provided to allow other investigators to repeat the work. Avoid repeating the details of procedures which have already been published elsewhere.

Results: The results should be presented as concisely as possible. Do not use tables *and* figures for presentation of the same data.

Discussion: The discussion section should be used for the interpretation of results. The results should not be repeated.

In some cases it might be desirable to combine results and discussion sections.

References: References should be given in the text by the surname of the authors and the year. *Et al.* should be used in the text when there are more than two authors. All authors should be given in the Reference section. In the Reference section the references should be listed alphabetically. See below for style to be used.

DEWALD, B., DULANEY, J.T., and TOUSTER, O. 1974. Solubilization and polyacrylamide gel electrophoresis of membrane enzymes with detergents. In *Methods in Enzymology,* Vol. xxxii, (S. Fleischer and L. Packer, eds.) pp. 82–91, Academic Press, New York.

HASSON, E.P. and LATIES, G.G. 1976. Separation and characterization of potato lipid acylhydrolases. Plant Physiol. *57,*142–147.

ZABORSKY, O. 1973. *Immobilized Enzymes,* pp. 28–46, CRC Press, Cleveland, Ohio.

Journal abbreviations should follow those used in *Chemical Abstracts.* Responsibility for the accuracy of citations rests entirely with the author(s). References to papers in press should indicate the name of the journal and should only be used for papers that have been accepted for publication. Submitted papers should be referred to by such terms as "unpublished observations" or "private communication." However, these last should be used only when absolutely necessary.

Tables should be numbered consecutively with Arabic numerals. The title of the table should appear as below:

Table 1. Activity of potato acyl-hydrolases on neutral lipids, galactolipids, and phospholipids

Description of experimental work or explanation of symbols should go below the table proper. Type tables neatly and correctly as tables are considered art and are not typeset. Single-space tables.

Figures should be listed in order in the text using Arabic numbers. Figure legends should be typed on a separate page. Figures and tables should be intelligible without reference to the text. Authors should indicate where the tables and figures should be placed in the text. Photographs must be supplied as glossy black and white prints. Line diagrams should be drawn with black waterproof ink on white paper or board. The lettering should be of such a size that it is easily legible after reduction. Each diagram and photograph should be clearly labeled on the reverse side with the name(s) of author(s), and title of paper. When not obvious, each photograph and diagram should be labeled on the back to show the top of the photograph or diagram.

Acknowledgments: Acknowledgments should be listed on a separate page.

Short notes will be published where the information is deemed sufficiently important to warrant rapid publication. The format for short papers may be similar to that for regular papers but more concisely written. Short notes may be of a less general nature and written principally for specialists in the particular area with which the manuscript is dealing. Manuscripts which do not meet the requirement of importance and necessity for rapid publication will, after notification of the author(s), be treated as regular papers. Regular papers may be very short.

Standard nomenclature as used in the engineering literature should be followed. Avoid laboratory jargon. If abbreviations or trade names are used, define the material or compound the first time that it is mentioned.

EDITORIAL OFFICES: DR. D.R. HELDMAN, COEDITOR, *Journal of Food Process Engineering,* National Food Processors Association, 1401 New York Avenue, N.W., Washington, D.C. 20005 USA; or DR. R.P. SINGH, COEDITOR, *Journal of Food Process Engineering,* University of California, Davis, Department of Agricultural Engineering, Davis, CA 95616 USA.

CONTENTS